Journal of Biomolecular NMR, 2 (1992) 109–136
ESCOM

J-Bio NMR 046

The solution conformation of sialyl-α(2→6)-lactose studied by modern NMR techniques and Monte Carlo simulations*

Leszek Poppe, Rainer Stuike-Prill, Bernd Meyer and Herman van Halbeek**

Complex Carbohydrate Research Center and Department of Biochemistry, The University of Georgia, 220 Riverbend Road, Athens, GA 30602, U.S.A.

Received 1 July 1991
Accepted 13 September 1991

Keywords: Oligosaccharide; Hydroxyl proton; Selective 3D NMR; Long-range {^{1}H,^{13}C} *J*-coupling; Metropolis Monte Carlo simulation

SUMMARY

We present a comprehensive strategy for detailed characterization of the solution conformations of oligosaccharides by NMR spectroscopy and force-field calculations. Our experimental strategy generates a number of interglycosidic spatial constraints that is sufficiently large to allow us to determine glycosidic linkage conformations with a precision heretofore unachievable. In addition to the commonly used {^{1}H,^{1}H} NOE contacts between aliphatic protons, our constraints are: (a) homonuclear NOEs of hydroxyl protons in H_2O to other protons in the oligosaccharide, (b) heteronuclear {^{1}H,^{13}C} NOEs, (c) isotope effects of O^{1}H/O^{2}H hydroxyl groups on ^{13}C chemical shifts, and (d) long-range heteronuclear scalar couplings across glycosidic bonds.

We have used this approach to study the trisaccharide sialyl-α(2→6)-lactose in aqueous solution. The experimentally determined geometrical constraints were compared to results obtained from force-field calculations based on Metropolis Monte Carlo simulations. The molecule was found to exist in 2 families of conformers. The preferred conformations of the α(2→6)-linkage of the trisaccharide are best described by an equilibrium of 2 conformers with Φ angles at −60° or 180° and of the 3 staggered rotamers of the Ω angle with a predominant *gt* conformer. Three intramolecular hydrogen bonds, involving the hydroxyl protons on C8 and C7 of the sialic acid residue and on C3 of the reducing-end glucose residue, contribute significantly to the conformational stability of the trisaccharide in aqueous solution.

INTRODUCTION

The interest in the 3D structure and dynamics of oligosaccharide moieties of glycoconjugates is intensifying as evidence of their biological functions increases (Cumming and Carver, 1987; Rade-

**Supplementary material available from the corresponding author:* Table containing values for the dihedral angles Φ, Ψ, Ω, Θ, and for bond angles τ, for the six lowest-energy conformations of sialyl-α(2→6)-lactose (1 page).

**To whom correspondence should be addressed.

macher et al., 1988; Ram et al., 1989; Carver et al., 1990; Homans, 1990a; Meyer, 1990; Yan and Bush, 1990; Meyer et al., 1991). Oligosaccharides present a particular challenge for solution conformation analysis, as they are made up of glycosyl residues with relatively rigid internal ('intraresidue') conformation, held together by much more flexible glycosidic linkages. The intraresidue conformations can be fairly well characterized by the measurement of vicinal aliphatic proton-proton coupling constants, but no such homonuclear scalar couplings across the glycosidic linkage are observed. Therefore, conformation analysis by NMR of oligosaccharides in solution has focused heavily (Bock, 1983; Cumming and Carver, 1987; Bush, 1988; Homans, 1990a) on the measurement of NOE effects or cross-relaxation rates between pairs of aliphatic protons, which are used as the internuclear distance gauge (Neuhaus and Williamson, 1989). For solution conformation analysis of oligosaccharides, unlike that of peptides and nucleotides (Wüthrich, 1986), the number of NOE contacts observed between aliphatic protons of adjacent residues is usually limited to one or two, and NOE interactions between such protons in nonadjacent residues are rare. Consequently, solution conformations of carbohydrates cannot be clearly defined based solely on those interglycosidic NOEs.

The accurate determination of the glycosidic torsional angles Φ and Ψ, and the Ω angle for exocyclic groups requires more rigorous NMR analysis. Also, the orientation of free hydroxyl groups relative to the glycosyl ring has been largely ignored thus far. Recently, we have shown that the number of structurally relevant homonuclear NOE interactions may be significantly augmented by taking exchangeable protons (mainly hydroxyl protons) into consideration, both in aqueous (Poppe and Van Halbeek, 1991a) and nonaqueous solution (Dabrowski and Poppe, 1989; Poppe et al., 1990a). Another potentially useful parameter for defining the glycosidic linkage conformation are the vicinal proton-carbon scalar coupling constants across the bond, which are related to the dihedral angles Φ and Ψ through an adapted Karplus equation (Karplus, 1959; Mulloy et al., 1988; Tvaroska et al., 1989). Recently, we introduced 2 new methods for ^{1}H-detected measurements of such couplings (Poppe and Van Halbeek, 1991c,d), enabling more rapid and accurate determination of $^3J_{CH}$. Their values, in combination with the aforementioned NOE effects, can now be utilized more readily for determination of the conformation of glycosidic bonds. Finally, heteronuclear NOE contacts may be useful in situations where one of the above methods fails, for example when the anomeric carbon is a quaternary carbon atom (Poppe and Van Halbeek, 1991b).

Evaluation of the constraints obtained from NMR analysis by force-field calculations of energetically favored conformations is required to obtain the 3D structure of oligosaccharides in solution (Bock, 1983; Homans et al., 1987; Cumming and Carver, 1987; Lemieux, 1989; Ram et al., 1989; Meyer, 1990). Several different force fields have been used for the calculation of the conformation of biologically relevant oligosaccharides (Thøgersen et al., 1982; Rasmussen, 1983; Scarsdale et al., 1988; Ha et al., 1988; Imberty et al., 1990; Homans, 1990b; Carver et al., 1990;

Abbreviations: DSS, sodium 4,4-dimethyl-4-silapentane-1-sulfonate; FID, free induction decay; Gal, D-galactose; Glc, D-glucose; GlcNAc, *N*-acetyl-D-glucosamine; NeuAc, *N*-acetyl-D-neuraminic acid (a sialic acid); GEGOP, geometry of glycoproteins; HOHAHA, homonuclear Hartmann–Hahn; HSQC, heteronuclear single-quantum coherence; MD, molecular dynamics; MMC, Metropolis Monte Carlo; NOE, nuclear Overhauser effect; NOESY, nuclear Overhauser spectroscopy; RF, radio-frequency; ROESY, rotating-frame NOE spectroscopy; SL, spin-lock; S6L, sialyl-α(2→6)-lactose; TOCSY, total correlation spectroscopy; TPPI, time-proportional phase incrementation.

Stuike-Prill and Meyer, 1990). Most theoretical studies thus far have focused on the calculation of local and global energy minima that are then correlated to experimental data. Because NMR spectroscopy yields time-averaged parameters, single-point calculations of local and global minima do not give the best representation of experimentally acquired data. However, incorporating the flexibility of oligosaccharides into the calculations can significantly improve the correlation between experimental and theoretical data (Carver et al., 1990; Homans, 1990a,b; Peters et al., 1991). Studies on the dynamics of oligosaccharides that have been published use either molecular dynamics (MD) (Brady, 1989; Edge et al., 1990; Homans, 1990b; Yan and Bush, 1990) or Metropolis Monte Carlo simulations (MMC) (Rees and Smith, 1975; Meyer et al., 1991; Peters et al., 1991).

Here we report specifically on the determination of the 3D structure of the trisaccharide NeuAcα(2→6)Galβ(1→4)Glc (S6L) in aqueous solution. A structurally related analogue of this trisaccharide, namely, NeuAcα(2→6)Galβ(1→4)GlcNAc, is found as the terminal entity on the carbohydrate chains of many sialylated glycoproteins and plays a role as a receptor in molecular and cellular interactions (Schauer, 1982; Rademacher et al., 1988). Our experimental analysis comprises measurements of $\{^1H,^1H\}$ NOE effects for aliphatic and hydroxyl protons (both in the rotating frame and in the laboratory frame), isotope effects of O^1H/O^2H hydroxyl groups on ^{13}C resonances, $\{^{13}C,^1H\}$ steady-state NOE measurements involving the quaternary anomeric carbon atom of the sialic acid residue, and measurements of $\{^1H,^1H\}$ and $\{^{13}C,^1H\}$ vicinal coupling constants. In addition, measuring anomerization effects ($\Delta\delta_{\alpha\beta}$) (i.e., differences in chemical shift of some of the ^1H and ^{13}C nuclei of the galactosyl and sialyl residues between the α and β anomer of the reducing trisaccharide) proved helpful. By tailoring the modern techniques of high-resolution NMR spectroscopy to the study of oligosaccharides, we could determine more than 25 structurally relevant constraints for sialyl-α(2→6)-lactose. The resulting 3D structural constraints were evaluated by Metropolis Monte Carlo (MMC) simulations at 300 K and 800 K using the GEGOP program (Stuike-Prill and Meyer, 1990) with a modified HSEA force field.

Preliminary accounts of this investigation were presented at the XIth International Symposium on Glycoconjugates, Toronto, Canada (Poppe and Van Halbeek, 1991f) and at the 10th International Meeting on NMR Spectroscopy, St. Andrews, Scotland (Van Halbeek and Poppe, 1991).

MATERIALS AND METHODS

NMR spectroscopy

Various samples of sialyl-α(2→6)-lactose (S6L, purchased from Biocarb) were prepared for NMR studies. They contained 20–50 mM solutions of deuterium-exchanged S6L in $D_2O/(CD_3)_2CO$, 9:1, v/v, and 20–50 mM solutions of S6L in mixtures of $H_2O/(CD_3)_2CO$, with compositions ranging from 10:1 to 3:1, v/v, and a 20 mM solution of S6L in a mixture of H_2O/D_2O, 1:1, v/v. The pH values of the solutions were 7.0 ± 0.5. The addition of $(CD_3)_2CO$ to the solutions allowed us to lower the sample temperature to 248 K. It is noteworthy that the effect of adding acetone to the aqueous solutions in the aforementioned composition ranges on the chemical shifts and exchange rates of hydroxyl protons is negligible as compared to the influence of temperature and pH of the solutions.

The NMR experiments were performed on a Bruker AM-500 spectrometer, equipped with an Aspect-3000 computer and BFX-5 linear amplifier, operating in the 'inverse mode' for the ^1H-de-

tected experiments, i.e., using the decoupler as the sole source of ^1H RF pulses. Homonuclear experiments were conducted using a 5-mm dedicated ^1H probe; for the heteronuclear (both ^{13}C- and ^1H-detected) experiments we used a 5-mm $\{^{13}C,^1H\}$ dual frequency probe with conventional geometry. The ^1H and ^{13}C spectra were referenced to internal DSS by setting the residual $(C\underline{H}D_2)CO(CD_3)$ signal to 2.204 ppm and the $(\underline{C}D_3)_2CO$ signal to 31.88 ppm, respectively.

Selective 1D and 2D HSQC spectra were obtained with the pulse sequence described previously (Poppe and Van Halbeek, 1991e):

$$\begin{array}{lccccccc} ^1H: & 90_x - \tau - & 180 - \tau - & SL_x & -90_y - \delta - & 180 - \delta - & 90_x - & Acq_{x,-x,-x,x} \\ ^{13}C: & & 180 & & 90_{x,-x} - & \Delta & -90_{x,x,-x,-x} & \end{array}$$

In the 1D HSQC experiment, designed to reveal one-bond connectivities between NeuAc side-chain carbons and protons, the ^{13}C carrier frequency was centered at the NeuAc C9 or C8 resonance. The delay τ was 1.5 ms, the spin-lock (SL) time was 5 ms, and δ was jittered randomly between 1 and 10 ms every 16 scans, for a total of 800 scans. The phase of the ^1H 180° pulses was alternated.

For the accurate measurement of long-range $^1H,^{13}C$ coupling constants, selective 1D HSQC experiments were performed with the first 180° ^1H pulse (a DANTE pulse train of 20 ms) applied to either the Gal H1 or the Glcα H1 resonance, while the corresponding Gal C5 and Glc C5 frequencies in the ^{13}C spectrum were selected by jittering of the delay δ. For measuring the Gal H1/C5 and Glcα H1/C5 couplings, the delays τ were 110 ms and 50 ms, respectively. A total of 3200 scans were accumulated for each spectrum, with acquisition time 1.5 s and relaxation delay 0.5 s.

In the 2D HSQC experiment, the ^{13}C carrier frequency was centered at the Glc C4 resonance. The ^{13}C 180° pulse was 2 ms long, while all ^1H pulses were hard. Quadrature detection in t_1 was obtained with TPPI (Marion and Wüthrich, 1983). The delay τ was 40 ms and the acquisition times t_2 and t_1 were 1.02 s (spectral width 2000 Hz, 4 K datapoints) and 0.1 s (spectral width 1000 Hz, 200 datapoints), respectively. After zero-filling in both dimensions, the final resolution was 0.5 Hz/pt and 3.9 Hz/pt. The relaxation delay was 0.7 s; 32 scans were accumulated per t_1 value.

The selective 3D homonuclear TOCSY-ROESY experiment (Sklenar and Feigon, 1990) used the following pulse sequence:

$$90_{\varphi 1} - 180_{\varphi 2} - \Delta - T_{\varphi 1+90} - MLEV17_{\varphi 1} - T_{\varphi 1+90} - t_1 - SL_{\varphi 1+90} - Acq_{\varphi 3}$$

where $\varphi_1 = 4x,4y,4(-x),4(-y)$; $\varphi_2 = (x,y,-x,-y), (y,-x,-y,x), (-x,-y,x,y), (-y,x,y,-x)$; and $\varphi_3 = (x,-x,x,-x), (y,-y,y,-y), (-x,x,-x,x), (-y,y,-y,y)$. The phases φ_1, φ_2 and φ_3 were incremented by 180°, after every 16 scans. T represents a short (3 ms) trim pulse. Quadrature detection in t_1 was obtained by TPPI and the ^1H carrier frequency was positioned at the Gal H1 resonance during the entire experiment. The 90° and 180° pulses were selective DANTE pulses (Morris and Freeman, 1978) with durations 20 and 40 ms, respectively. The 90° pulse train $(\alpha° - \tau - \alpha° - \tau)_n$ had the first and last interpulse delay set to $\tau/2$ (Wu et al., 1989); the delay Δ was 13 ms. The TOCSY (MLEV-17) and ROESY (SL) mixing times were 77 ms and 140 ms, respectively. The spin-lock was generated by a series of short (ca. 14°) pulses; the average field strength $<\gamma B_1>$ was 1.5 kHz. The acquisition times in t_2 and t_1 domains were 0.68 s (spectral width 3000 Hz, 4 K datapoints) and 0.11 s (spectral width 1100 Hz, 256 datapoints), respectively. After zero-filling, the fi-

nal resolution was 0.73 Hz/pt and 4.3 Hz/pt. The relaxation delay between consecutive scans was 1.1 s; 32 scans were accumulated per t_1 increment.

The 1D ROESY experiments (Bax and Davis, 1985) were performed with direct subtraction of the reference FID every 8 scans, for a total number of 800 scans. The selective 180° DANTE pulse was 10 ms long. The mixing time (100–200 ms) consisted of a series of short pulses, with the carrier positioned at the selectively inverted proton resonance; the average field strength $<\gamma B_1>$ for spin-lock was 1.9–3.0 kHz. The acquisition time and relaxation delay were 1.3 and 1.1 s, respectively.

The heteronuclear 1D NOE difference spectra were obtained with selective presaturation of ^1H resonances using the DANTE-z pulse sequence (Boudot et al., 1989) for saturation of one resonance at a time, or applying two interleaved DANTE pulse trains (Geen et al., 1989; Poppe and Van Halbeek, 1991b) for simultaneous irradiation of 2 resonances. One of the trains consisted of short pulses with rotating phase (in 60° steps for the simultaneous irradiation of NeuAc $H3_{ax}$ and $H3_{eq}$, and in 30° steps for the Gal H6R and H6S protons); the second train consisted of the same short pulses with phase inversion of the even-numbered pulses every 8 scans together with the receiver phase, in analogy to the DANTE-z scheme (Poppe and Van Halbeek, 1991b). The interpulse delays were 164 μs for the NeuAc $H3_{ax}/H3_{eq}$ experiments and 220 μs for the Gal H6R/H6S experiment. The presaturation and relaxation times were 6 s each; 1600 scans were accumulated per spectrum. The CYCLOPS phase cycle (Hoult and Richards, 1975) was applied to the ^{13}C read pulse and the receiver.

For the experiments in H_2O solution, the following pulse sequence was used (Sklenar and Bax, 1987):

$$\text{presat. (or sel.inv.)} - 90_{\varphi 1} - \Delta_1 - 90_{\varphi 1} - \Delta_2 - 90_{\varphi 2} - 2\times\Delta_1 - 90_{\varphi 2} - \Delta_2 - SL_{\varphi 3} - Acq_{\varphi 4}$$

The phases were as described previously (Poppe and Van Halbeek, 1991a) and the values for delays Δ_1 and Δ_2 are in the legend to Fig. 7. Presaturation, selective inversion and spin-locking were accomplished with DANTE pulse trains. The 1D TOCSY, 1D ROESY, and 1D NOE difference spectra of S6L in H_2O were recorded with direct subtraction of the reference FID every 16 scans for a total of 160–320 scans, with 1.3 s acquisition time and 1.1 s relaxation delay, respectively.

Force-field calculations

Theoretical conformational studies were performed with the force-field program GEGOP (Stuike-Prill and Meyer, 1990). The energy of the oligosaccharide conformers was calculated using a modified HSEA force field. The original HSEA force field includes potential energy functions for Van der Waals interactions and a torsional term for the *exo*-anomeric effect (Thøgersen et al., 1982). In the GEGOP program, a new parameterization of the *exo*-anomeric effect based on recent ab-initio calculations on dimethoxymethane on a STO6-31G* level (Wiberg and Murcko, 1989), supplemented by our own calculations on the same level, has been implemented. Also, a torsional potential for the rotation of the C5–C6 bond has been included in the current version of the program. The parameterization was derived from MNDO calculations of D-glucose and D-galactose (Stuike-Prill and Meyer, 1991). Furthermore, the glycosidic bond angle is changed during optimizations or dynamical studies of the geometry of the molecule.

The conformation of the oligosaccharide is defined by the torsion angles Φ(H1′–C1′–O1′–C4)

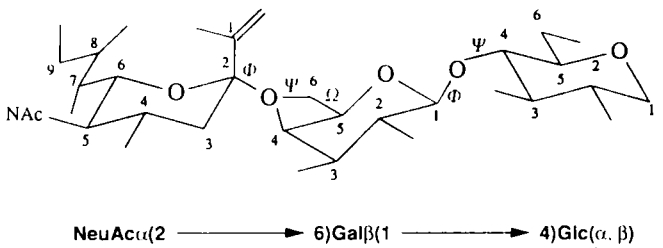

Fig. 1. Schematic structure of sialyl-α(2→6)-lactose (S6L). The numbering of the carbon atoms and their substituents is indicated. The torsional angles Φ and Ψ around the (1→4) glycosidic bond are defined as follows: Φ(H1′–C1′–O1′–C4) and Ψ(C1′–O1′–C4–H4). The angles Φ and Ψ around the (2→6) glycosidic linkage are defined as Φ(C1′–C2′–O2′–C6) and Ψ(C2′–O2′–C6–C5), while Ω is taken as (O2′–C6–C5–O5) (see also diagram in Table 4).

and Ψ(C1′–O1′–C4–H4) of the Gal(1→4)Glc glycosidic bond, the torsion angles Φ(C1′–C2′–O2′–C6) and Ψ(C2′–O2′–C6–C5) of the NeuAc(2→6)Gal bond, and the angle Ω(O2′–C6–C5–O5) of the C5–C6 bond (see Fig. 1). The atomic coordinates of the monosaccharide residues were taken from X-ray structure analysis. The coordinates for hydrogens were generated according to geometrical criteria. During the calculation the dihedral angles of the glycosidic linkages and of the exocyclic bonds including those of the hydroxyl groups as well as the glycosidic bond angles were varied, whereas the bond angles of the pyranose rings and all bond lengths of the monosaccharide residues ($^4C_1$ conformation for the Gal and Glc residues, $^2C_5$ for the NeuAc residue) were kept constant.

Three Metropolis Monte Carlo simulations (Metropolis et al., 1953) of the dynamics of S6L were performed. Two runs with 500 000 steps each were conducted using an MMC temperature parameter of 300 K with different starting conformations of the α(2→6)-linkage, and a third run of 1 000 000 steps was performed at 800 K. The intervals for the variations of the dihedral angles were chosen between 10° and 20° to achieve an acceptance rate of 30–50%. During the simulations all dihedral angles in the molecule and certain distances between atoms were sampled in each MMC step and stored for further processing.

Ensemble average coupling constants, distances, and rotamer populations were derived from these sampled data. For $^3J_{HH'}$ scalar couplings, we used the Karplus equations as parametrized by Haasnoot, De Leeuw and Altona ('HLA equation') (Haasnoot et al., 1980):

$$J_{H5H6R} = 13.22\cos^2\theta - 0.99\cos\theta - 6.4\cos^2(25.87-\theta) - 0.96\cos^2(7.96+\theta) + 2.61$$

$$J_{H5H6S} = 13.22\cos^2\theta - 0.99\cos\theta - 0.96\cos^2(\theta+7.96) - 3.2\cos^2(25.87-\theta) - 3.2\cos^2(25.87+\theta) + 2.61$$

For $^3J_{CH}$ couplings across glycosidic linkages we adopted the equation (Tvaroska et al., 1989):

$$^3J_{CH} = 5.7\cos^2\theta - 0.6\cos\theta + 0.5$$

For the other heteronuclear couplings we adopted the equation (Spoormaker and De Bie, 1978):

$$^3J_{CH} = 3.09 - 0.38\cos(\theta - 5.53) + 2.57\cos2(\theta - 5.53)$$

The averaged distances were calculated according to $< r^{-3} >^{-1/3}$.

The calculations were performed on either DECstations 5000 or DECsystems 5500. For molecular graphics we used the SYBYL software package on a Silicon Graphics 4D/220 GTX. The traces and contour plots from the Monte Carlo simulations were generated with the PV-Wave software package on a DECsystem 5500.

TABLE I

^1H AND ^{13}C CHEMICAL SHIFTS FOR SIALYL-α(2→6)-LACTOSE[a] IN D_2O/ACETONE-d_6

	Residue (in anomer of trisaccharide)[b]			
Nucleus	α-NeuAc	β-Gal	Glc(β)	Glc(α)
H1		4.442	4.678	5.235
H2		3.564(α)	3.323	3.611
		3.556(β)		
$H3_{ax}$	1.759	3.681(α)	3.664	3.859
		3.677(β)		
$H3_{eq}$	2.732			
H4	3.672	3.948	3.647	3.632
H5	3.874	3.850	3.624	3.964
H6R		4.001(α)	3.810	3.890[c]
		3.996(β)		
H6S	3.733	3.643	3.964	3.872[c]
H7	3.582			
H8	3.900			
H9R	3.658			
H9S	3.884			
NAc CH_3	2.044			
C1	175.810(α)	105.573(α)	97.991	94.154
	175.796(β)	105.590(β)		
C2	102.602(α)	73.118	76.060	73.376
	102.597(β)			
C3	42.436	74.680	77.000	73.967
C4	70.691	70.887(α)	81.945	82.097
		70.873(β)		
C5	54.147	76.030	76.955	72.269
C6	74.847	65.929	62.562	62.410
C7	70.722			
C8	74.149			
C9	65.072			
NAc CH_3	24.310			
NAc CO	177.239			

[a] Data were acquired in $D_2O/(CD_3)_2CO$ (9:1, v/v) at pD 7.0 ± 0.2 and 296 K. ^1H chemical shifts are referenced to internal DSS, with residual acetone-d_5 as the internal standard. ^{13}C chemical shifts are referenced to DSS, with the acetone-d_6 methyl carbon as the internal standard.

[b] Under the given conditions, the S6L solution contains a mixture of the α and β anomer of the trisaccharide, in the molar ratio of 3:5.

[c] Assignments may have to be interchanged.

RESULTS

NMR experiments

The aliphatic ^1H resonances of S6L were assigned (see Table 1) by 1D TOCSY (Braunschweiler and Ernst, 1983) (also known as 1D HOHAHA; Subramanian and Bax, 1987) experiments applying selective 180° DANTE and double-DANTE pulses (Geen et al., 1989; Poppe and Van Halbeek, 1991b). Our assignments were basically the same as those reported for S6L by Platzer et al. (1989). The hydroxyl proton resonances of S6L were assigned by the same technique, with a 1-1 echo pulse sequence (Sklenar and Bax, 1987) implemented for water suppression as described previously (Poppe and Van Halbeek, 1991a). The assignments for the OH signals that could not be assigned by scalar coupling techniques are based on 1D NOE experiments (see Table 2, footnotes h,i). The ^{13}C spectrum of S6L was then assigned on the basis of an HMQC experiment (Müller,

TABLE 2

^1H CHEMICAL SHIFTS (δ), SCALAR COUPLING CONSTANTS (*J*), TEMPERATURE COEFFICIENTS (κ), AND LINE BROADENINGS ($\Delta\nu_{1/2}$) FOR HYDROXYL AND AMIDO PROTONS OF SIALYL-α(2→6)-LACTOSE[a] IN H_2O/ACETONE-d_6

Residue	Nucleus	δ[b]	*J*[c]	κ[d]	$\Delta\nu_{1/2}$[e]
α-NeuAc	OH4	6.496[f]	5.3	−6.4	0.60
	NH5	8.33	9.5	−2.9	<0.1
	OH7	5.635 (α)[g]	9.3	−4.2	0.15
		5.616 (β)[g]			
	OH8	6.437[h]	<2	−2.8	0.15
	OH9	5.883[f]	5.9	−7.5	0.35
β-Gal	OH2	6.664 (α)[g]	5	−6.7	0.35
		6.662 (β)[g]			
	OH3	6.200	6	−6.8	0.45
	OH4	6.117	5.9	−7.0	0.35
Glc(β)	OH1	8.027	5	−5.7	0.35
	OH2	6.592	5.5	−6.7	0.45
	OH3	5.628	2.5	−2.8	0.15
	OH6	6.029	6.0	−7.7	0.80
Glc(α)	OH1	7.284[i]	<2	−5.0	0.90
	OH2	6.200	6	−6.8	0.45
	OH3	5.532	2.5	−2.8	0.15
	OH6	5.958	6	−7.8	0.70

[a] Data were acquired in $H_2O/(CD_3)_2CO$ (3:1, v/v) at pH 7.2 ± 0.2.

[b] H chemical shifts are in ppm at 248 K, referenced to internal DSS, with acetone-d_5 as the internal standard.

[c] *J* values are in Hz.

[d] Temperature coefficients are in ppm/K × 10^3.

[e] Line broadening $\Delta\nu_{1/2}$ in (Hz/K × 10^3), calculated as pure exchange broadening over the temperature interval from 248 K to 268 K.

[f] These assignments were inadvertently interchanged in a previous study (Poppe and Van Halbeek, 1991a).

[g] The S6L solution contains a mixture of the α and β anomer in the ratio of 3:5.

[h] Assigned in our previous study (Poppe and Van Halbeek, 1991a).

[i] Assigned on the basis of its NOE to H1 of Glc(α).

1979; Lerner and Bax, 1987). The ^{13}C chemical shifts of S6L (Table 1) are consistent with previously reported assignments (Berman, 1984).

The 1D TOCSY spectra enabled us to accurately measure the majority of the $^3J_{HH'}$ scalar coupling constants of S6L (Poppe et al., 1989). The J values pertinent for conformational analysis were converted into H-C-C'-H' dihedral angles through the HLA equation (Haasnoot et al., 1980). Thus, the Gal and Glc residues were confirmed to be in the $^4C_1$ chair conformation, whereas the NeuAc residue adopts the $^2C_5$ chair conformation. For the NeuAc side chain, the coupling constants $^3J_{H6H7}$ (= 1.7 Hz) and $^3J_{H7H8}$ (= 9.5 Hz) were obtained in a straightforward way. However, the remaining coupling constants, $^3J_{H8H9S}$ and $^3J_{H8H9R}$, were difficult to extract from either 1D TOCSY spectra or a 1D COSY spectrum with chemical-shift selective filter (Poppe and Van Halbeek, 1991b), due to the strong overlap of the NeuAc H8 and H9S signals. Fortunately, the NeuAc C8 and C9 resonances in the ^{13}C spectrum (Table 1) are well separated. This feature allowed us to obtain undistorted, first-order multiplets of H9S and H9R in a modified 1D HSQC experiment (Fig. 2) (Otting and Wüthrich, 1988; Poppe and Van Halbeek, 1991c). From this experiment we determined $^3J_{H8H9R}$ to be 6.4 Hz and $^3J_{H8H9S}$, 2.4 Hz; the assignment of the prochiral protons H9R and H9S was reported previously (Brown et al., 1975; Acquotti et al., 1990). Thus, we estimated the molar ratio of the three staggered conformers *gt*:*gg*:*tg* around the NeuAc C8–C9 bond to be 0.5:0.0:0.5.

Glycosidic linkage conformations

To determine the conformation of the (2→6)-glycosidic linkage between NeuAc and Gal in terms of the dihedral angles Φ, Ψ and Ω (Fig. 1), or more precisely, in terms of populations of the angles among all rotational states, we assumed that the exocyclic group of the Gal residue can occur in three staggered rotamers around C5–C6 (*gt*, *gg*, and *tg*, corresponding to Ω is 60°, −60° and 180°, respectively). Before the populations of the staggered rotamers (p_{gt}, p_{gg}, and p_{tg}) could be calculated from the vicinal coupling constants $^3J_{H5H6R}$ and $^3J_{H5H6S}$, the unambiguous assign-

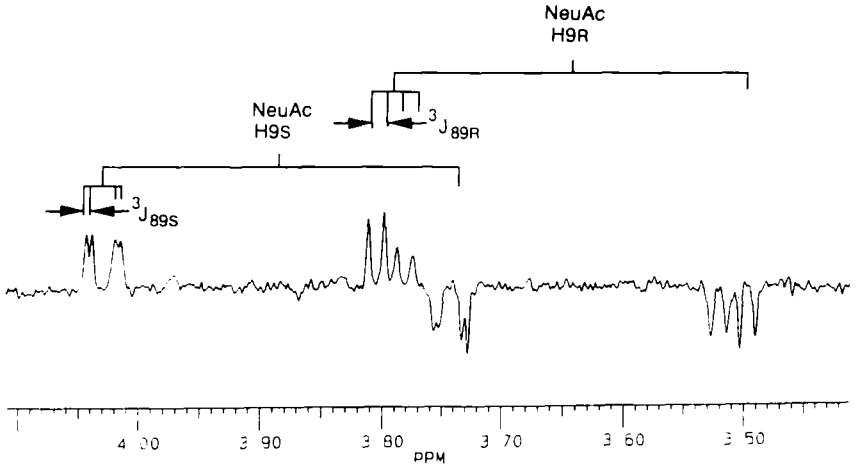

Fig. 2. Selective 1D {^1H,^{13}C} HSQC spectrum of sialyl-α(2→6)-lactose. Through selective irradiation of NeuAc C9 in the ^{13}C spectrum, correlations between C9 and H9R and also between C9 and H9S are visualized. The spectrum was recorded for a solution of S6L in D_2O/$(CD_3)_2CO$, 9:1 (v/v) at ambient temperature.

ment of the prochiral protons Gal H6R and H6S was required. We based our assignment of Gal H6R and H6S on so-called 'NOE labelling' (Homans et al., 1986; Poppe et al., 1989) taking into account the spatial proximity of H6R and H6S protons to H4 in the Gal residue. Because of the severe spectral overlap in the regions where the signals of Gal H6R and H6S are observed, it was not possible to assign H6R and H6S from 2D ROESY (NOESY) spectra. Therefore, we resorted to a selective homonuclear 3D TOCSY-ROESY NMR experiment (Sklenar and Feigon, 1990), in which magnetization was first transferred by the TOCSY mechanism from the H1 proton of the Gal residue to its H4, and subsequently in a ROESY step to protons Gal H6S and H6R. The resulting selective 3D spectrum is shown in Fig. 3. Only a strong interaction between H4 (δ 3.948) and $H6^{H}$ (δ 3.643) is observed. The interaction between H4 and $H6^{L}$ (δ 4.00) (where H and L stand for high- and low-field shifts, respectively) is intrinsically much weaker, and additionally quenched by the indirect NOE effect between H4/$H6^{H}$/$H6^{L}$, which in ROESY spectra has opposite phase to the direct effects (Farmer et al., 1987). In an analogous selective 3D TOCSY-NOESY experiment with the same mixing time (spectrum not shown), we observed a negative NOE effect between Gal H4 and $H6^{L}$. We then repeated the selective 3D TOCSY-ROESY and TOCSY-

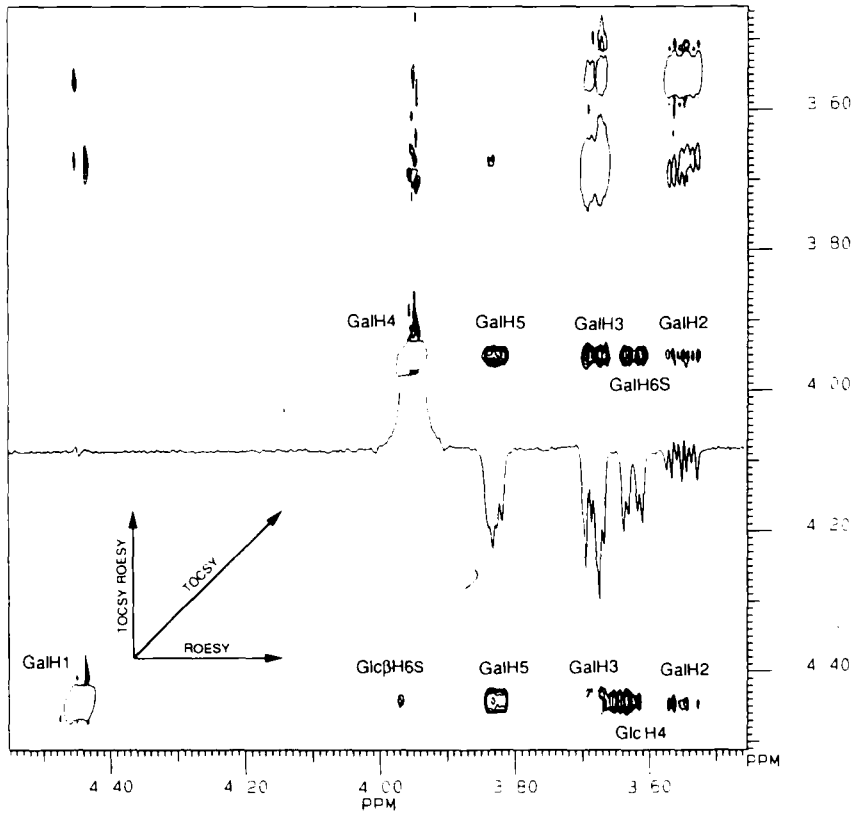

Fig. 3. Selective 3D TOCSY-ROESY spectrum of sialyl-α(2→6)-lactose. The spectrum was recorded for a solution of S6L in D_2O $(CD_3)_2CO$, 9:1 (v/v) at ambient temperature. Through selective irradiation of Gal H1, the ROESY, TOCSY, and TOCSY-ROESY (or back-transfer) connectivities are obtained in a 2D cross section, as indicated. Positive signals are drawn with one contour, negative signals in multiple levels.

TABLE 3
AVERAGE DISTANCES (IN Å) AND VICINAL COUPLING CONSTANTS J (IN Hz) FOR SIALYL-α(2→6)-LACTOSE IN AQUEOUS SOLUTION

Atom pair	Measured NMR value[a]	Monte Carlo simulated (at 300 K)[b]	
		Family I[c]	Family II[c]
NeuAc/Gal			
$H3_{ax}$ H6R	3.3	4.35	2.35
$H3_{ax}$ H6S	3.3	4.63	2.53
$H3_{ax}$/H4	> 5	6.34	4.78
$H3_{eq}$/H6R	5	4.54	3.37
$H3_{eq}$ H6S	4	4.33	3.84
$H3_{eq}$ H5	5	5.15	4.62
$H3_{eq}$ H4	> 5	6.53	5.62
OH8 H6R	3.5	3.58	6.56
OH8 H6S	> 4	5.07	5.67
O7 Glc O3	3[d]	3.43	5.64
C2 H6R	2.6	2.56	2.79
C2 H6S	> 2.6[e]	2.90	2.67
$^3J_{C2\,H6S}$	1.8 ± 0.2	1.22	3.42
$^3J_{C2\,H6R}$	2.8 ± 0.2	3.95	3.01
Gal/Gal			
$^3J_{H5\,H6R}$	8.5 ± 0.2	9.25	6.46
$^3J_{H5\,H6S}$	3.7 ± 0.2	3.97	4.17
$^3J_{C4\,H6R}$	2.9 ± 0.5	2.48	2.39
$^3J_{C4\,H6S}$	1.8 ± 0.5	1.75	3.07
H4 H6R	3.3	3.02	2.88
H4 H6S	2.6	2.65	2.75
Gal/Glc			
H1 H4	2.5	2.39	2.48
H1 H6S	3.5	2.72	2.69
H6R OH3	3.5	4.17	4.39
$^3J_{H1\,C4}$	4.2 ± 0.2	2.58	2.08
$^3J_{C1\,H4}$	5.1 ± 0.4	5.07	5.22
H6R O3[f]		4.28	4.43
H6S O3		5.09	5.01

[a] The distances were evaluated from the formula: $r_{ij} = r_{kl}(I_{kl}/I_{ij})^{1/6}$, where I_{ij}, I_{kl} are the integrated signal intensities; I_{kl} corresponds to the reference interaction. For ROESY spectra the intensities were scaled by the offset-dependent factor: $(\sin\theta_i \sin\theta_j)^{-2}$, in which $\theta_i = \arctan(\Omega_i / \langle \gamma B_1 \rangle)$; Ω_i represents the offset from the carrier and $\langle \gamma B_1 \rangle$ the effective field strength in Hz. The precision of distances is roughly $0.1 \times r$.

[b] Simulated distances were calculated according to $\langle r^{-3} \rangle^{-1/3}$.

[c] Family I corresponds to the Metropolis Monte Carlo simulation started from glycosidic angle Φ of the (2→6)-linkage set to −60°; for family II the pertinent angle was set to 180°.

[d] This value corresponds to the hydrogen bond from NeuAc OH7 to Glc O3, discussed in the text.

[e] For the detailed discussion of this result see text.

[f] The $\Delta\delta_{\alpha\beta}$ effect was observed only for the prochiral H6R proton which is closest to O3 of the Glc residue.

NOESY experiments at 270 K, i.e., under slow-tumbling rate conditions ($\omega\tau_c > 1$); the combined results of these experiments allowed for a rather precise estimation of the averaged H4/H6^L and H4/H6^H distances (Table 3) despite the complication of spin diffusion between H6^L and H6^H (Fejzo et al., 1989). The close spatial proximity of Gal H4 and H6^H, in conjunction with the large vicinal coupling $^3J_{H5H6^L}$ (8.5 Hz) allowed us to unequivocally assign the prochiral Gal protons H6^L as H6R and H6^H as H6S (see diagram on top of Table 4). Table 4 lists the relative populations of *gt*, *gg* and *tg* conformers around the Gal C5–C6 bond at 3 different temperatures. The populations were first calculated from vicinal couplings through the HLA equation; they were then verified independently on the basis of ΔG values obtained from population distributions at the lowest temperature (277 K). Despite the relatively large error margins it can be concluded that both calculations are consistent; they show the same trend in the change of *J* couplings with temperature. The temperature dependence of the vicinal coupling constants (Table 4) rules out the occurrence of a single rotamer around the C6–C5 bond (Homans et al., 1986).

To determine the allowed ranges of Φ and Ψ values for the (2→6)-linkage we measured a number of dipolar contacts and vicinal couplings which are included in Table 3. The interproton dipolar contacts were obtained from 1D ROESY experiments (Bothner-By et al., 1984; Bax and

TABLE 4

ROTAMER DISTRIBUTION OF THE EXOCYCLIC GROUP, AND VICINAL COUPLING CONSTANTS J_{56}, IN THE GALACTOSYL RESIDUE OF SIALYL-α(2→6)-LACTOSE AT DIFFERENT TEMPERATURES[a]

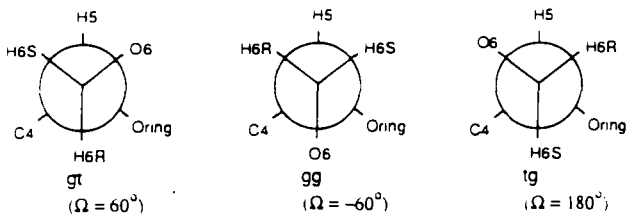

Population	277 K	294 K[b]		350 K[b]	
p_{gt}	0.74 ± 0.03	0.71 ± 0.03	0.71 ± 0.05	0.64 ± 0.02	0.66 ± 0.04
p_{gg}	0.18 ± 0.03	0.20 ± 0.03	0.19 ± 0.02	0.22 ± 0.02	0.22 ± 0.02
p_{tg}	0.08 ± 0.03	0.08 ± 0.03	0.10 ± 0.03	0.14 ± 0.02	0.12 ± 0.03
J_{56R}	8.5 ± 0.2	8.3 ± 0.2	8.3 ± 0.2	7.8 ± 0.2	7.9 ± 0.2
J_{56S}	3.7 ± 0.2	3.8 ± 0.2	3.8 ± 0.2	4.2 ± 0.2	3.9 ± 0.2

[a] Calculated from the vicinal coupling constants J_{56R} and J_{56S} using the HLA equation and, alternatively (values in the right-hand columns at 294 K and 350 K) from ΔG° values. The ΔG° values were obtained from the formula: $\Delta G^\circ_{ij} = -RT\ln(p_j/p_i)$, where R is the gas constant, T = 277 K and populations were calculated from the HLA equation; $\Delta G^\circ_{tg\,gt} = 5.24 \pm 0.9$ kJ/mol, $\Delta G^\circ_{gg\,gt} = 3.2 \pm 0.3$ kJ/mol, $\Delta G^\circ_{tg\,gg} = 1.9 \pm 0.5$ kJ/mol. The errors were estimated from the standard error propagation law.

[b] The values in the left columns for 294 K and 350 K were obtained from *J* values, those in the right columns from ΔG° values, respectively.

Davis, 1985) (Fig. 4). The rotating-frame NOE measurements clearly showed their dramatic advantage in sensitivity over laboratory-frame measurements (Fig. 4c shows an ROE effect below 0.1% between Gal H4 and NeuAc $H3_{eq}$). The laboratory-frame NOE method was found unsuitable for S6L at ambient temperature ($\omega\tau_c \sim 1$). Moreover, at low temperatures ($\omega\tau_c > 1$), the direct and indirect NOE effects were only clearly distinguishable in the rotating frame.

Heteronuclear intra- and interglycosidic NOE contacts were measured as described previously (Poppe and Van Halbeek, 1991b). The steady-state $^{13}C\{^1H\}$ NOE difference spectra (Figs. 5a,c,e) were obtained by simultaneous saturation of both methylene resonances (NeuAc $H3_{ax}/H3_{eq}$ in traces a and c, and Gal H6R/H6S in trace e) followed by subtraction of spectra where only one methylene proton (NeuAc $H3_{eq}$, $H3_{ax}$ and Gal H6S in a, c, e, respectively) was saturated. By eliminating the destructive three-spin effect (Poppe and Van Halbeek, 1991b), the NeuAc C2 NOE dif-

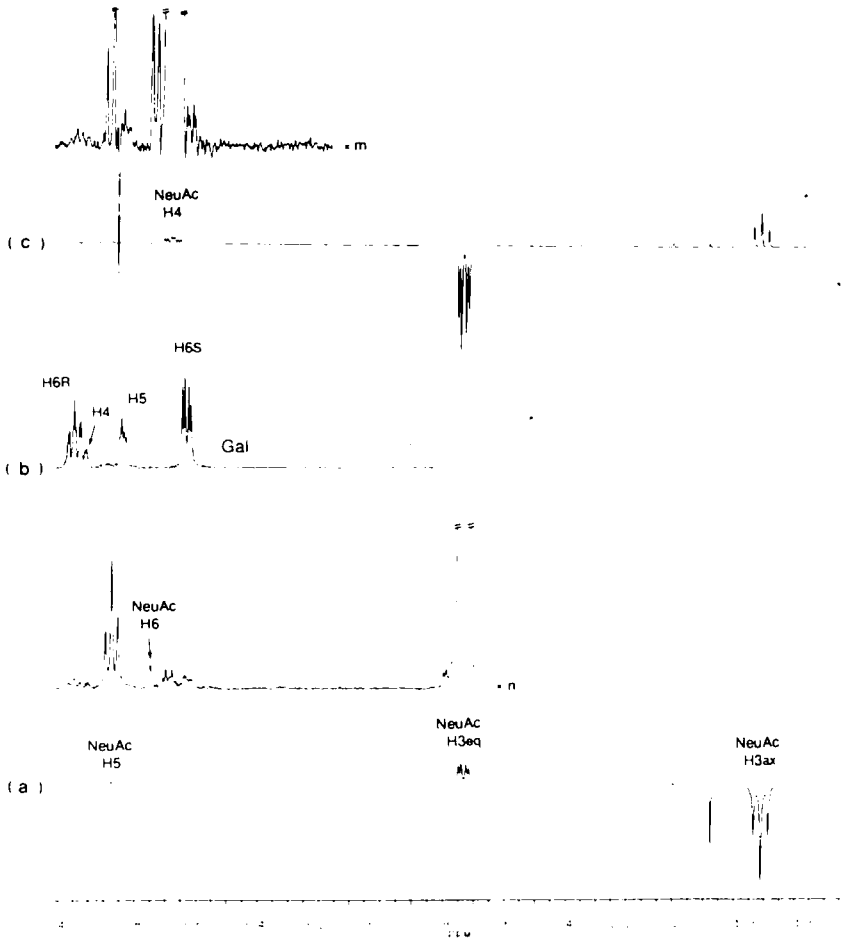

Fig. 4. Selective 1D ROESY spectra of sialyl-α(2→6)-lactose obtained after selective inversion of (a) NeuAc $H3_{ax}$ and (c) NeuAc $H3_{eq}$. The mixing time was 150 ms. The antiphase pattern of the NeuAc H5 signal on trace (c) originates from antiphase terms evolved during the mixing time (Bothner-By and Shukla, 1988). (b) Control 1D TOCSY spectrum obtained after selective inversion of the low-field component of the Gal H6R signal. The mixing time was varied between 30 and 100 ms.

ference signals were enhanced compared to those observed upon single selective saturation of NeuAc $H3_{ax}$ (Fig. 5b), NeuAc $H3_{eq}$ (Fig. 5d) or Gal H6R (Fig. 5f), respectively. The largest NOE enhancements were observed for the NeuAc $H3_{ax} \leftrightarrow H3_{eq} \leftrightarrow C2$ spin system (see legend to Fig. 5), as expected for the nuclear geometry where both protons are close in space to the carbon nucleus and to each other. These NOEs were used for calibration of $^{13}C,^{1}H$ internuclear distances. The experiment aimed at detecting interglycosidic NOEs between the Gal H6R and/or H6S and NeuAc C2 gave only a small increase (1.00:0.93) in intensity of the NeuAc C2 signal (compare traces e and f in Fig. 5). This observation strongly suggests that the average distance between Gal

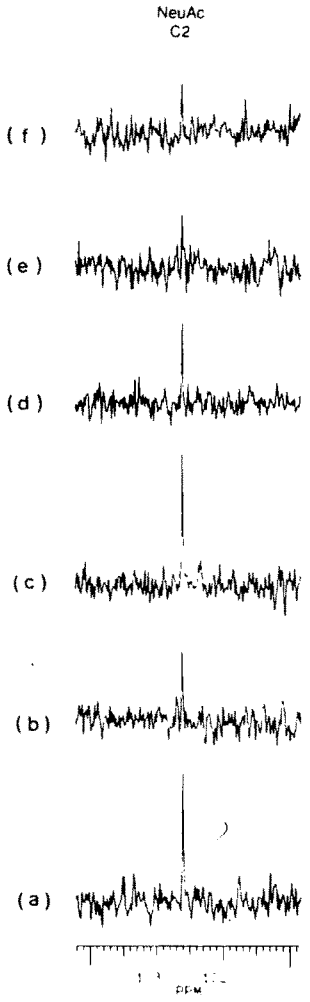

Fig. 5. Selective 1D $^{13}C\{^{1}H\}$ NOE difference spectra obtained with (a) simultaneous presaturation of NeuAc $H3_{ax}$ and $H3_{eq}$, followed by subtraction of selective saturation of $H3_{eq}$, (b) selective presaturation of NeuAc $H3_{ax}$ only, (c) simultaneous presaturation of NeuAc $H3_{ax}$ and $H3_{eq}$, followed by subtraction of selective saturation of $H3_{ax}$, (d) selective presaturation of NeuAc $H3_{eq}$ only, (e) double-selective presaturation of Gal H6R and H6S, followed by subtraction of selective saturation of H6S, and (f) selective presaturation of Gal H6R only. The increases in intensity of the NeuAc C2 signal were measured to be: 1:0.63 (b vs. a), 1:0.57 (d vs. c), and 1:0.93, (f vs. e), respectively.

H6S and NeuAc C2 is larger than the averaged distance Gal H6R–NeuAc C2. This information was valuable since the H6S/C2 interaction could not be measured directly because of the overlap of the Gal H6S and NeuAc H4 and H6 resonances in the spectrum. However, any spurious NOE effects on C2 resulting from NeuAc H4 and H6 saturation are cancelled in the difference experiment (Fig. 5e). In other words, the steady-state heteronuclear NOE difference experiment allowed us to measure the Gal H6R–NeuAc C2 interaction, while simultaneously enabling us to 'spy' the Gal H6S–NeuAc C2 contact (see also Poppe and Van Halbeek, 1991b).

In addition to the through-space Gal H6–NeuAc C2 contacts, we measured Φ and Ψ torsion angle constraints, namely, the interglycosidic vicinal scalar couplings $^3J_{C2H6R}$ and $^3J_{C2H6S}$ (see Table 3) by the modified HSQC techniques described previously (Poppe and Van Halbeek, 1991c,d).

With respect to the Galβ(1→4)Glc linkage, 1D ROESY experiments such as those shown in Fig. 4 clearly revealed Gal H1–Glc H4 and Gal H1–Glcβ H6S contacts (spectra not shown). The ROE contact between Gal H1 and Glcβ H6R, and those between Gal H1 and Glcα H6R,S as well, partially overlap with the strong Gal H1–H5 interaction. The constraints are included in Table 3.

For the Glcβ hydroxymethyl group we measured $^3J_{H5H6R} = 4.6$ Hz and $^3J_{H5H6S} = 2.2$ Hz, where the assignment of Glc H6R and H6S was based on Ohrui et al. (1985). Thus, the rotamer population ratio *gt:gg:tg* calculated for Glcβ through the HLA equation was 0.3:0.7:0. The values measured for the heteronuclear $^3J_{C4H6S}$ (5.2 ± 0.5 Hz) and $^3J_{C4H6R}$ (2.0 ± 0.5 Hz) are in reasonable agreement with the values one would calculate (by the Spoormaker equation) from the *gt:gg:tg* ratio 0.3:0.7:0, namely, $^3J_{C4H6S} = 4.6$ Hz, and $^3J_{C4H6R} = 1.5$ Hz. The large Glcβ C4/H6S coupling is clearly visible in the selective 2D HSQC spectrum of S6L (Fig. 6) (Poppe and Van Halbeek, 1991e). This spectrum also shows the heteronuclear Gal H1–Glc C4 multiplets, separated for both anomers of the trisaccharide. The heteronuclear vicinal coupling constants through the Galβ(1→4)Glc linkage are included in Table 3.

Intramolecular hydrogen bonds

The spectral parameters of the hydroxyl protons (Fig. 7), in particular their temperature coefficients and line widths, were used to establish the occurrence of intramolecular hydrogen bonds. The significantly smaller exchange rates and temperature coefficients for NeuAc OH8, NeuAc OH7, and Glc OH3, as well as their extreme values of scalar coupling constants (Table 2) suggest the involvement of these three OH groups in hydrogen bonds. The intraresidue hydrogen bond between NeuAc OH8 and the ring oxygen and/or the carboxyl group of the NeuAc residue has

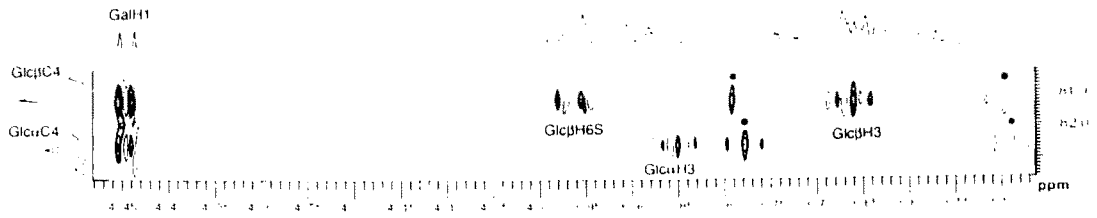

Fig. 6. Expansion of a ^{13}C-selective 2D {^{1}H,^{13}C} HSQC spectrum of sialyl-α(2→6)-lactose, showing antiphase multiplets with respect to long-range heteronuclear couplings to Glc C4 (α and β). Positive signals are drawn with one contour. The asterisks indicate the antiphase Glc H4(α) and H4(β) multiplets due to one-bond couplings to the C4 atoms.

been reported before (Poppe and Van Halbeek, 1991a). From the data listed for the S6L OH3 proton of the Glc residue, both in the α and β anomer of the trisaccharide (Table 2), we inferred its involvement in a stable hydrogen bond, probably interresidual to the O5 atom of the Gal residue, analogous to the hydrogen bond observed between Glc OH3 and Glc' O5 for cellobiose in the crystalline state (Chu and Jeffrey, 1968). The same hydrogen bond was previously postulated for (sialyl) oligosaccharides in aprotic solvents (Casu et al., 1966; Poppe et al., 1990a,b). Additional

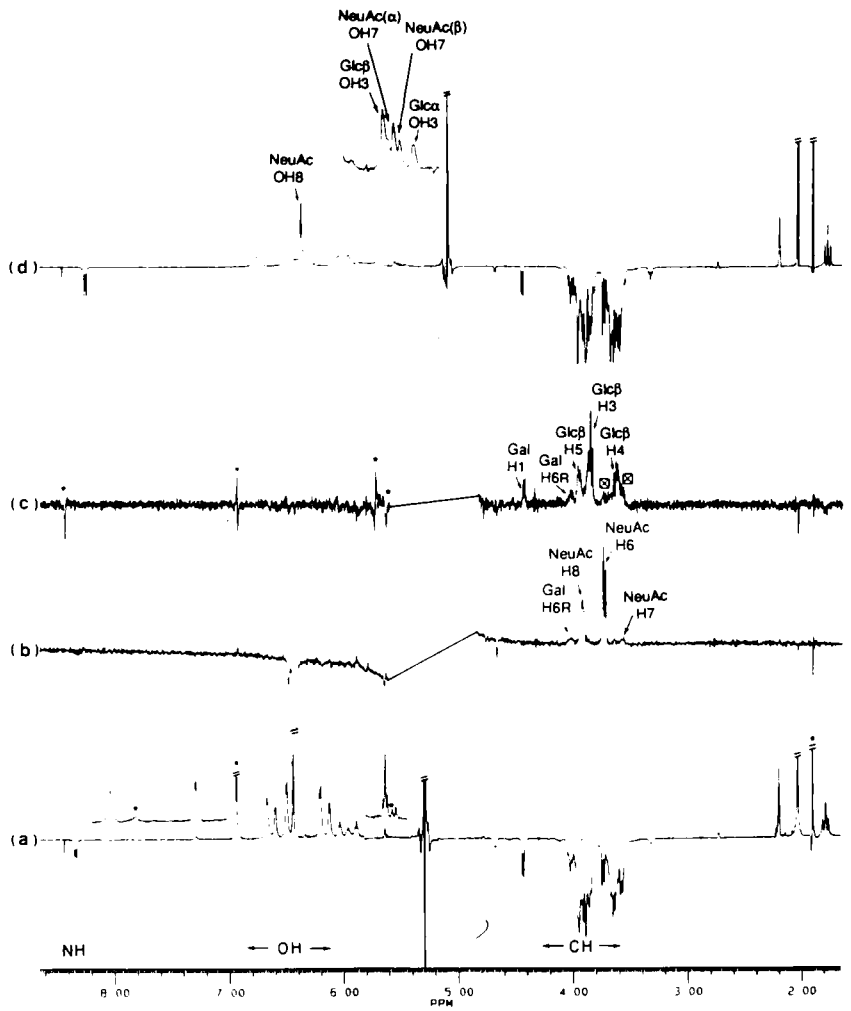

Fig. 7. ^{1}H NMR spectra of sialyl-α(2→6)-lactose in $H_2O/(CD_3)_2CO$, 4:1 (v:v) solution. Traces (a), (b) and (c) were obtained at 248 K and trace (d) at 272 K. The spectral parameters as described in the 'Materials and methods' section are as follows: (a) and (d): 1D spectra with $\Delta_1 = 0.4$ ms, $\Delta_2 = 100$ μs, spin-lock = 2 ms. The low-field and high-field insets were taken from the spectra recorded with $\Delta_1 = 0.17$ ms and 0.8 ms, respectively, showing the spectral regions not excited on the main trace due to the modulation of the excitation power (Poppe and Van Halbeek, 1991a). (b) 1D ROESY spectrum obtained after selective inversion of NeuAc OH8 resonance with a DANTE pulse train of 60 ms duration; the spin-lock time was 170 ms. (c) 1D NOE difference spectrum with selective presaturation of the Glcα OH3 resonance during 0.5 s. The Glc H5 and Gal H1 resonances appeared predominantly due to spin diffusion. The signals marked with an asterisk appear due to the spurious irradiation of the proximal NeuAc OH7 resonance.

evidence for this hydrogen bond was obtained from an NOE experiment (Fig. 7c), where the strong interaction between Glcα OH3 and Glc H4, and the weak contact between Glc OH3 and Galβ H6R further confirmed that the Glc OH3 proton points toward the Gal ring oxygen, at least for a significant population of the molecules.

Additional qualitative information on the solution structure of S6L was obtained from the observation of so-called anomerization effects, that is, chemical shift differences $\Delta\delta_{\alpha\beta}$ between the 2 anomers of the trisaccharide, for nuclei belonging to the Gal and NeuAc units. These effects, as chemical shifts, can not easily be predicted, but, if observed, may indicate the spatial proximity of the nucleus in question to the anomeric center of the reducing Glc residue. For example, the $\Delta\delta_{\alpha\beta}$ effect was detected for the Gal H3, Gal C1 and NeuAc C1 and C2 atoms (Table 1), but it was absent for the Gal H1 atom. Interestingly, the Gal C4 signal was found doubled in the anomeric intensity ratio, too; this is not attributable to close spatial proximity of the Gal C4 atom and the Glc OH1 group. Most surprisingly, a very large $\Delta\delta_{\alpha\beta}$ effect (9.3 Hz) was observed for the NeuAc OH7 proton (Table 2). This strongly suggests that this proton is in close proximity to the Glc reducing end. Among other hydroxyl protons, the anomerization effect was only detected for the Gal OH2 proton. In addition, the NeuAc OH7 proton shows the same characteristic features (line width, temperature coefficient) as the NeuAc OH8 and Glc OH3 protons (Table 2). This means that NeuAc OH7 is involved in a stable intramolecular hydrogen bond as well. Taking into account that the $^3J_{OH7H7}$ coupling is large (9.3 Hz) (Table 2), molecular model examination suggests that this hydrogen bond is formed either directly to O3 or/and O2 of the Glc residue, or indirectly through a water molecule. Independent evidence for the arrangement of NeuAc OH7 and Glc O3/O2 within hydrogen bond distance was obtained by potential energy calculations (see below). Unlike in G_{M1} (Acquotti et al., 1990), the NeuAc OH7 proton in S6L is not (at least not for a significant proportion of the time) involved in a hydrogen bond with the carbonyl oxygen of the *N*-acetyl group. The vicinal coupling constants of NeuAc OH7 (see Table 2) and the relatively weak NOE between NeuAc OH7 and H7 (spectrum not shown) indicate that the OH7 and H7 protons are *trans* oriented, an arrangement that is unfavorable for $CH_3NC=O:::OH7$ hydrogen bond formation.

In order to obtain additional evidence for the intramolecular hydrogen bonds in S6L, we studied extensively the deuterium isotope effects on ^{13}C chemical shifts (Reuben, 1984; Christofides et al., 1986). Our findings on S6L imply that at low temperatures (248 K–268 K) at neutral pH values (pH 7.0 ± 0.5), the exchange of S6L hydroxyl protons in water is slow enough to observe short-range deuterium isotope shifts of carbon resonances. These effects are most pronounced for those carbons which bear *N*-acetamido or hydroxyl groups involved in stable intramolecular hydrogen bonds. Figure 8 shows ^{13}C spectra of S6L in 50% H_2O/50% D_2O (v/v) solution at various temperatures. At the lowest temperature, only the signals of NeuAc C5, NeuAc C=O of NAc, NeuAc C8, NeuAc C7 and Glc C3 show clear splitting due to deuterium isotope effects. Within each pair of signals the high-field component originates from the deuterated molecules. All remaining hydroxyl-bearing carbon resonances show only line broadening, no splitting of their resonances. The ^1H spectrum of S6L in 50% H_2O/50% D_2O (v/v) recorded at 278 K is shown in Figs. 8d,e. As expected, the NeuAc NH, NeuAc OH8, NeuAc OH7 and Glc OH3 resonances are the least exchange broadened among those of the labile protons. Assuming a simple model of exchange between two sites: C-O-H⇔C-O-D with equal populations, we estimated the exchange rates from the coalescence points. For NeuAc OH8, NeuAc OH7 and Glc OH3 protons the exchange

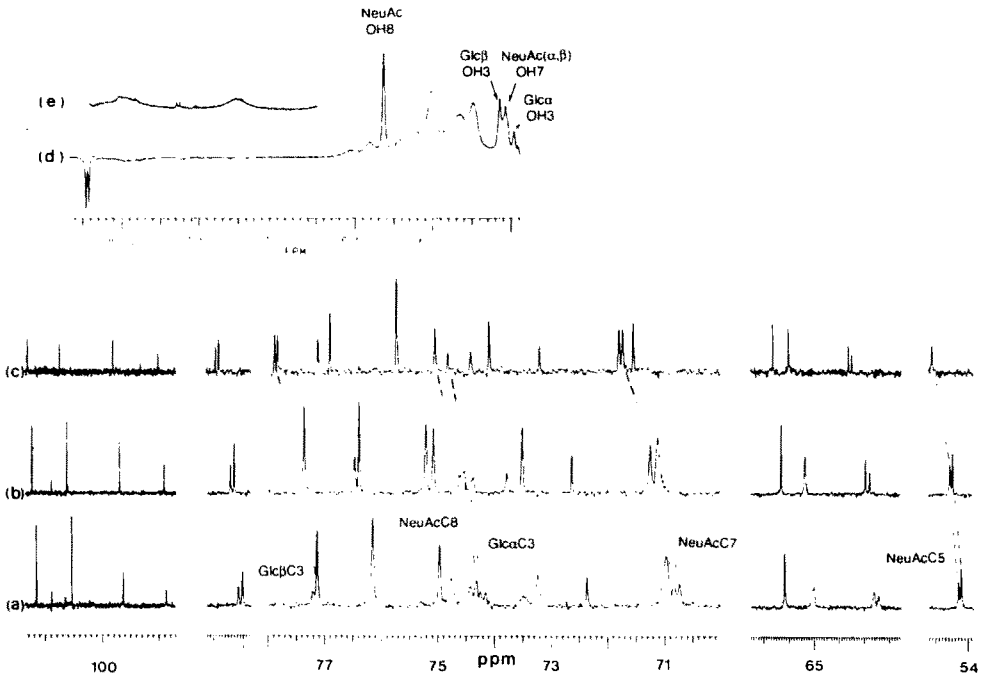

Fig. 8. 1D ^{1}H-decoupled ^{13}C spectra of S6L in 50% H_2O 50% D_2O (v v) at 274 K (a), 293 K (b), and 320 K (c). Only the carbon resonances that are split due to the deuterium isotope effect are marked. (d) and (e) Expanded OH-proton region of the 1D ^{1}H 1-1 echo spectrum of S6L in 50% H_2O 50% D_2O solution, obtained at 278 K as in Fig. 7a; spectra d and e were recorded with $\Delta_1 = 0.4$ ms and 0.19 ms, respectively.

rates are close to 27 s^{-1} at 294 K and pH 7.5. This corresponds to a free energy of activation ΔG^* on the order of 64 kJ/mol (obtained through the Arrhenius law). Exchange rates of this magnitude are unusual for carbohydrates (compare the recent studies of glucose in aqueous solution by Hills, 1991), and further support the existence of stable intramolecular hydrogen bonds.

Computer simulations

The experimental distance and torsion angle constraints gathered for S6L (Table 3) did not allow determination of the 3D structure without their evaluation by minimum energy calculations. For the simulations we adopted a modified HSEA force field (Lemieux et al., 1980; Stuike-Prill and Meyer, 1990), which allowed for extensive sampling of the conformational space. (The dihedral angles for S6L in its global minimum, and for the following 5 local minimum energy conformers, are listed in the supplementary material.) Using Monte Carlo simulations based on the Metropolis algorithm, which take shapes of the energy wells and barriers between wells into account, we calculated populations of the local minima, and thus, the NOE averaged distances and averaged scalar coupling constants, listed in Table 3.

In order to uniformly sample the conformational space of S6L, we started our Monte Carlo simulations at 800 K. At this temperature, the molecule can overcome energy barriers which are known to be overestimated in force-field calculations. The distribution of the dihedral angles Φ,

Ψ, and Ω of the glycosidic linkages at 800 K is shown in population plots (Figs. 9a–d). The populations are shown in 2D contour plots of the total populations projected out of a multidimensional space into a 2D area. The 1D projections of the populations are shown at the top and left of

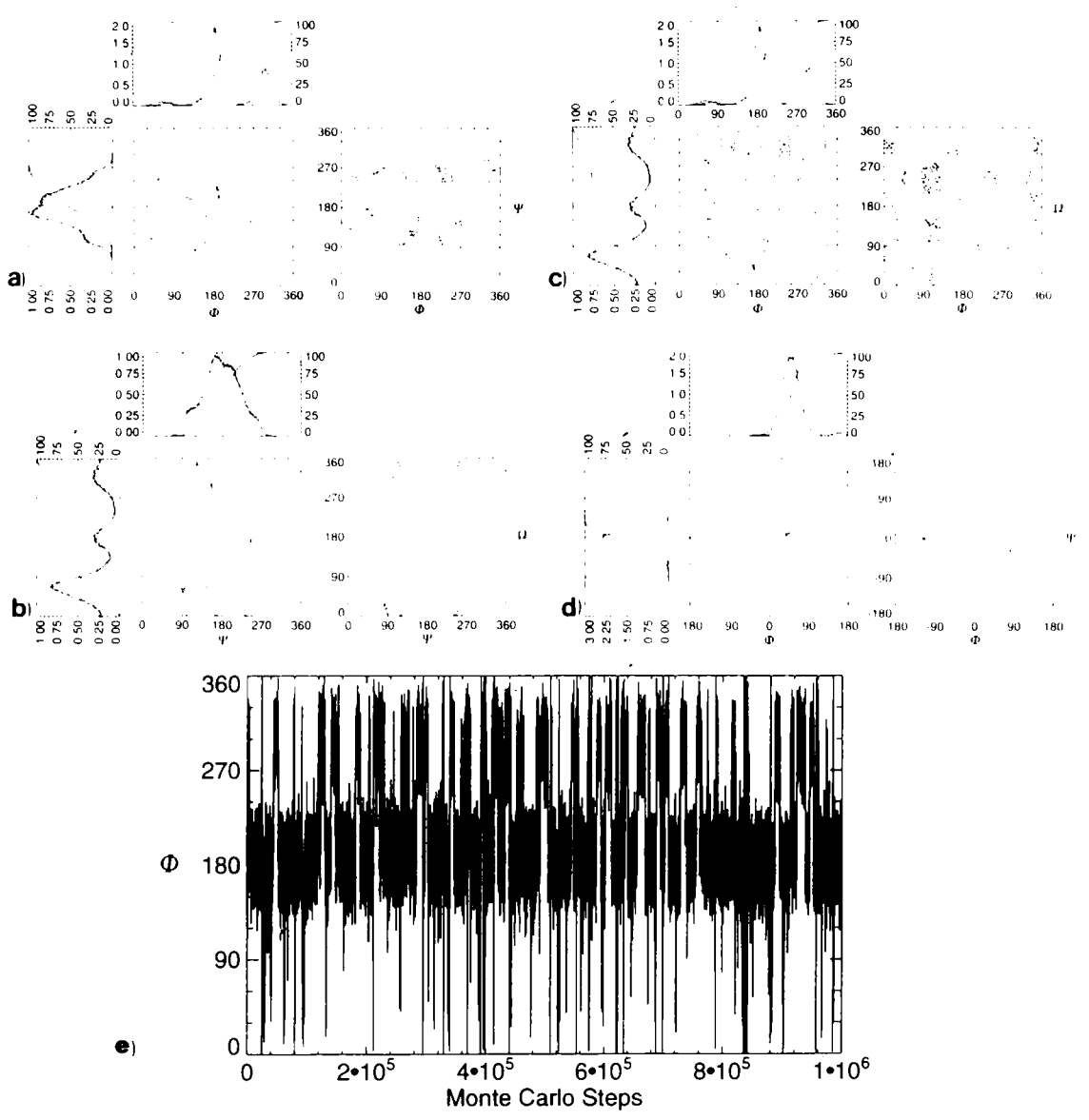

Fig. 9. Results of Metropolis Monte Carlo simulations (1 000 000 steps at 800 K) of sialyl-α(2→6)-lactose. (a) Population plot (left) and ΔG plot (right) for the Φ,Ψ pair of the (2→6)-linkage. (b) Population plot (left) and ΔG plot (right) for the Ψ,Ω pair of the (2→6)-linkage. (c) Population plot (left) and ΔG plot (right) for the Φ,Ω pair of the (2→6)-linkage. (d) Population plot (left) and ΔG plot (right) for the Φ,Ψ pair of the (1→4)-linkage. The populations are shown in 2D contour plots of the total populations projected out of a multidimensional space into a 2D area. The 1D projections of the populations are shown at the top and left of the contour plots. Populations are given in % relative to the highest populated conformer. (e) The trace of the glycosidic torsional angle Φ of the (2→6)-linkage.

the contour plots. The populations were converted into ΔG° values by applying Boltzmann statistics; the ΔG° plots are also shown in Figs. 9a–d. In contrast to calculations of local energy minima which yield only enthalpy values, the MMC simulations include implicitly the entropy. The simulations at 800 K revealed 2 major local minima for the $\alpha(2\rightarrow6)$-linkage centered around Φ values of -60° and 180°, a broad distribution of the Ψ angle around 180°, and three minima around the staggered rotamers of the Ω angle with values of -60°, 60°, and 180° (see Figs. 9a,b,c). The $\beta(1\rightarrow4)$-linkage shows only one major minimum, at Φ/Ψ $60^\circ/0^\circ$, with a small side minimum at $160^\circ/0^\circ$ (see Fig. 9d).

The flexibility of the individual dihedral angles of S6L is listed in Table 5. The ranges over which the dihedral angles varied clearly illustrate that all angles, except the C5–N1 angle of the *N*-acetamido group, have covered the whole conformational space during the MMC simulation at 800 K. The large values indicate that several rotations around the corresponding bond occurred during the simulation. The trace of the dihedral angle $\Phi_{(2\rightarrow6)}$ as a function of the MMC step shows that frequent transitions between the 2 most populated minima occur (Fig. 9e). This is essential for the analysis of the population equilibrium of the Φ angle (see below).

During the simulation at 800 K the NeuAc side chain preferred the extended zigzag conformations along the C6–C7, C7–C8, and C8–C9 bonds (see the average values of the side-chain angles of the NeuAc residue in Table 5). The C6–C7 bond remained almost entirely in the extended conformation, whereas the C7–C8 bond showed a distribution of 0.50:0.25:0.25 for the *gt*, *gg*, and *tg*

TABLE 5
PARAMETERS OF THE MMC CALCULATION OF SIALYL-$\alpha(2\rightarrow6)$-LACTOSE AT 800 K. GIVEN ARE THE STARTING ANGLES, THE AVERAGE ANGLES AND THE TOTAL RANGES COVERED DURING THE MMC SIMULATIONS

Residue Angle[a]	Start	Average	Range
NeuAc			
Φ	177	−145	2345
Ψ	156	179	249
Θ_{C6C7}	178	164	326
Θ_{C7C8}	−176	−178	1405
Θ_{C8C9}	53	−176	9747
Θ_{N1C5}	0	10	122
Θ_{C1C2}	16	−44	2094
τ	118	119	23
Gal			
Φ	54	54	303
Ψ	0	−5	193
Ω_{C6C5}	−39	147	4808
τ	117	118	24
Glc			
Ω_{C6C5}	−65	14	3947

[a] The glycosidic torsional angles Φ, Ψ and Ω are defined in Fig. 1. The NeuAc side-chain angles are denoted Θ. The glycosidic bond angles are denoted τ.

conformers, respectively. The terminal hydroxymethyl group occupied *gt*, *gg* and *tg* positions in the ratio 0.50:0.25:0.25, which is different from the estimations based on NMR experiments (vide supra). The distribution of the Ω angle for the α(2→6)-linkage obtained at 800 K is 0.44:0.40:0.16 for *gt*, *gg* and *tg* conformers, respectively.

With the largest barrier occurring between the 2 energy minima with $\Phi_{(2\rightarrow6)}$ −60° and 180°, we started MMC simulations at 300 K for these 2 rotamers. Two families of structures resulted from the MMC simulations at 300 K (see Fig. 10). The structures with $\Phi_{(2\rightarrow6)}$ −60° as starting value are

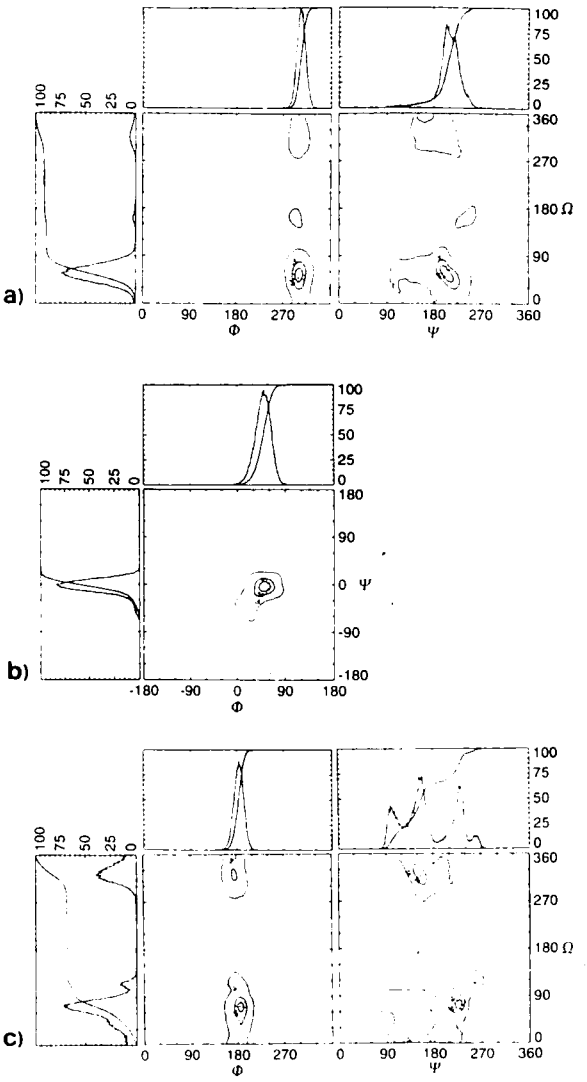

Fig. 10. Population plots for sialyl-α(2→6)-lactose obtained from Metropolis Monte Carlo simulations at 300 K. (a) Φ/Ω and Ψ/Ω plots for the (2→6)-linkage; (b) Φ/Ψ plot for the (1→4)-linkage. The starting conformation for the calculations in (a) and (b) had $\Phi_{(2\rightarrow6)}$ at −60°. (c) Φ/Ω and Ψ/Ω plots for the (2→6)-linkage where the calculations were started from a conformer with $\Phi_{(2\rightarrow6)} = 180°$. The linkage population plot for the (1→4)-linkage, when starting from $\Phi_{(2\rightarrow6)} = 180°$, is virtually identical to that in (b).

designated family **I**, the ones resulting from $\Phi_{(2\rightarrow6)}$ 180° are denoted family **II**. In Fig. 10, traces a and c show that, although the barrier between $\Phi_{(2\rightarrow6)}$ −60° and 180° could not be overcome at 300 K, all other degrees of freedom are in equilibrium at 300 K. Therefore the ensemble average distances and coupling constants are representative for each of the 2 local minima (Table 3).

The Boltzmann distribution between families **I** and **II** calculated at 800 K (where the two families of conformations are in thermal equilibrium) is about $p_I:p_{II}=0.32:0.63$. Under the assumption that the entropies of the individual populations are similar, an apparent ratio $p_I:p_{II}=0.13:0.87$ at 300 K was deduced. The *gt*, *gg*, *tg* distribution of the Ω angle for the α(2→6)-linkage at 300 K equals 0.89:0.09:0.02 for family **I** structures, and 0.67:0.31:0.02 for family **II** structures.

DISCUSSION

We have deduced the preferred conformations of sialyl-α(2→6)-lactose in aqueous solution by combining the results of 1D, 2D, and 3D NMR experiments (tailored to the conformation analysis problems of carbohydrates) with our force-field calculations. The selective 3D TOCSY-ROESY NMR experiment (Fig. 3) provided the unambiguous assignment of the prochiral protons Gal H6R and H6S. It is worth noting that the strong overlap of the Gal H6R and H6S proton signals with those of the H6R and H4 protons of the β-Glc residue would not have been alleviated by a conceptually similar 2D experiment called TORO (TOCSY-ROESY) (Kessler et al., 1988; Poppe and Dabrowski, 1989). Our assignments of the Gal H6R and H6S, based on NOE-labeling, match those obtained by diastereoselective deuteration for several sialyl-disaccharides, including NeuAcα(2→6)Gal (Ohrui et al., 1991).

Critically important interproton distances were obtained through sensitive 1D ROESY experiments (Fig. 4). The number of NOE effects we detected across the α(2→6)-linkage by this method (Table 3) was essential to the evaluation of the MMC-predicted conformation of this linkage. In a study of the conformation of NeuAcα(2→6)Galβ(1→4)GlcNAcβ(1→N)Asn by means of 2D $^1H,^1H$ NOESY and theoretical (HSEA) calculations, Breg et al. (1989) did not detect any NOE contacts between the NeuAc residue and the rest of the molecule. Our 1D ROESY studies also helped us avoid misinterpretations that could easily occur in analogous NOESY experiments for systems with proximal proton pairs like NeuAc $H3_{ax}$, $H3_{eq}$ and Gal H6R, H6S in S6L. On the other hand, in ROESY experiments we had to ensure that there would be no interference from Hartmann–Hahn effects. We minimized those effects by a judicious choice of the carrier frequency and the spin-lock field strength; the magnitudes of the Hartmann–Hahn effects can also be estimated under the two-spin approximation (Bax, 1988; Bothner-By and Shukla, 1988).

Isotope shift effects proved very helpful for assessing OH groups involved in hydrogen bonds (Fig. 8). Although not novel, studies of these effects by other investigators (Lemieux and Bock, 1984; Reuben, 1984; Christofides et al., 1986) were performed in DMSO solution in order to eliminate the chemical exchange of labile protons. To our knowledge, our efforts are the first that have been successful in observing isotope shift effects in pure aqueous solution, where chemical exchange phenomena severely restrict their study.

When evaluating the results of our conformation studies on S6L, most of the experimental parameters (Table 3) are in qualitative agreement with the predominance of structure family **I** over family **II**. This is best illustrated by comparing the *relative* magnitudes of NeuAc C2–Gal H6R

and NeuAc C2–Gal H6S NOE interactions and the $^3J_{C2,H6R}$ and $^3J_{C2,H6S}$ scalar couplings for family **I** and family **II** structures with the results of the calculations. For family **I** structures these coupling constants are well-reproduced by the calculations, while family **II** structures show a trend exactly opposite to the values predicted. Type **I** structures show a small scatter of interglycosidic torsional angles, particularly of the Ψ and Ω angles around the (2→6)-linkage (see Fig. 10a). The set of torsional angles in type **I** structures keeps the NeuAc O7/Glc O3 atom pair at a distance short enough (see Table 3) to support the experimental evidence for the NeuAc OH7:::Glc O3 hydrogen bond. In contrast, structures of type **II** show a large scatter of the Ψ and Ω angles around the (2→6)-linkage (see Fig. 10c) and thus do not account for a short average distance for the NeuAc O7/Glc O3 atom pair.

The most significant discrepancy between simulation and experiment was observed for the $^3J_{\text{Gal H1-Glc C4}}$ coupling constant (Table 3). The measured value (4.2 Hz) seems to be too large for angle Φ to be close to 60° most of the time, as predicted by the simulation. The ensemble average value from the MMC simulation is calculated to be 2.6 Hz. We thought one explanation for this discrepancy may lie in our interpretation of the experimental result: the parameterization of the Karplus equation (Tvaroska et al., 1989) may be inaccurate. To check the validity of this parameterization, we measured long-range, intraresidue $^1H,^{13}C$ coupling constants in order to arrive at a

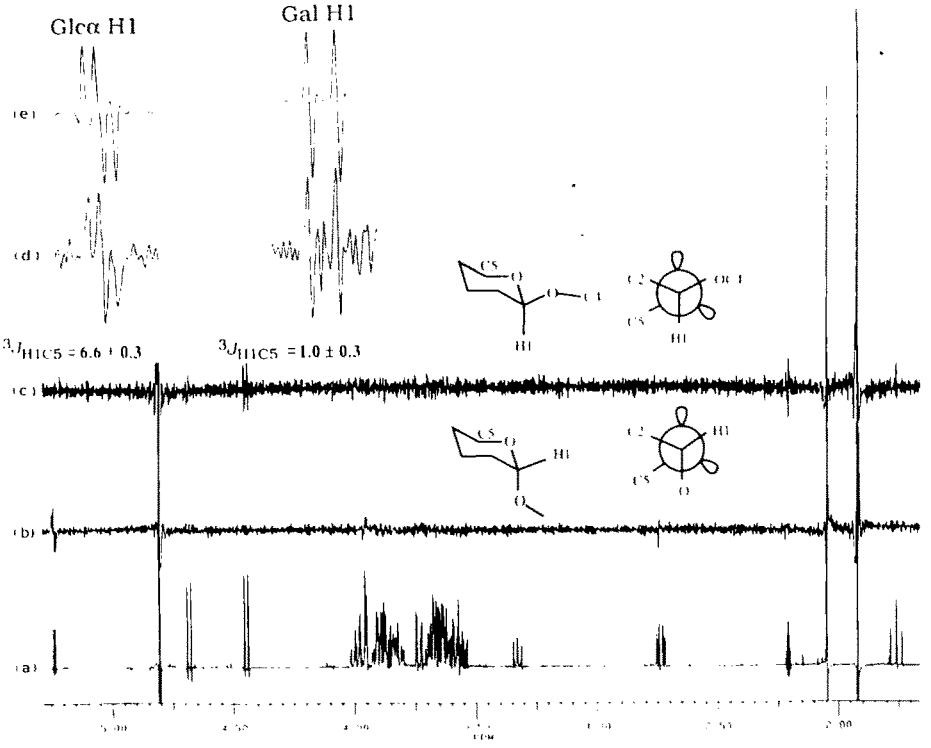

Fig. 11. (a) Reference ^1H NMR spectrum of S6L in D_2O. (b) and (c) Selective 1D HSQC spectra of S6L in D_2O solution, showing the Glcα H1 and Gal H1 multiplets arising due to the long-range $^1H,^{13}C$ coupling to C5 within the respective residues. The expanded H1 multiplets are shown in trace (d). For comparison, the theoretical multiplets are depicted in trace (e); they were obtained by subtracting a copy of the spectrum shifted by J from trace (a).

gauge for the interglycosidic dihedral angles independent of the Karplus equation. Note that the arrangement of the C5 and H1 atoms in the β-Gal residue is *gauche* ($\theta = 60^\circ$), but for the α-Glc residue it is *trans* ($\theta = 180^\circ$) (see diagrams in Fig. 11). The 1D HSQC spectra (Fig. 11) revealed that the $^3J_{C5H1}$ values for β-Gal and α-Glc are 1.0 and 6.6 Hz, respectively. Thus, the interglycosidic $^3J_{Gal\ H1\text{-}Glc\ C4} = 4.2$ Hz indicates that the Φ angle for the Galβ(1→4)Glc linkage should be significantly smaller or larger, for a significant proportion of the time, than the values ($60 \pm 20^\circ$) appearing on the contour plot of Fig. 10b.

The coupling constants $^3J_{Gal\ H1\text{-}Glc\ C4}$ and $^3J_{Gal\ C1\text{-}Glc\ H4}$ observed for the β(1→4)-linkage in S6L are virtually the same as the values obtained for lactose (Poppe and Van Halbeek, 1991d). This observation suggests that the attachment of NeuAc in α(2→6)-linkage to Gal has negligible influence on the β(1→4) glycosidic bond conformation, and contradicts the conclusions by Berman (1984) based on ^{13}C chemical shifts alone. Furthermore, the $^3J_{HH'}$ coupling constants in the NeuAc C7–C8–C9 side chain, as well as the long-range coupling constant $^4J_{C2\ H7}$ (1.5 Hz) (Poppe and Van Halbeek, 1991c), appeared the same for NeuAcα(2→6)Galβ(1→4)Glc as for NeuAcα-(2→3)Galβ(1→4)Glc (Poppe, unpublished). The stable intramolecular hydrogen bond involving the NeuAc OH8 group was also shown to be independent of the type of linkage in which sialic acid is involved (Poppe and Van Halbeek, 1991a). Thus, we conclude that the conformation of the sialic acid side chain does not depend on the type of linkage, c.q., the proximity of other residues (compare the results obtained for G_{M1} by Acquotti et al., 1990). Again, this contradicts the conclusions drawn from the analysis of ^{13}C chemical shift data alone (Berman, 1984).

Careful examination of the data compiled in Table 3 led us to conclude that sialyl-α(2→6)-lactose in aqueous solution can adopt conformations of both type **I** and type **II**. Structures of type **I** are stabilized by hydrogen bonds, namely, NeuAc OH7:::Glc O3 and Glc OH3:::Gal O5, while structures of type **II** appear to gain free energy from entropy terms associated with the flexibility of the (2→6)- and (1→4)-glycosidic linkages. It is tempting to speculate that the predominant solution structures of S6L are those of type **I**, which have an interresidue NeuAc OH7:::Glc O3 hydrogen bond. However, it is by no means a straightforward procedure to estimate the ratio in which types **I** and **II** occur in solution. The dynamics of interconversion of the 2 forms is fast on the NMR time scale, that is, fast enough to average the NMR spectrum. If interconversion is slower than the molecular tumbling, the ensemble average NOE effects or the equivalent average distances can be calculated from the values obtained individually for the 2 types of structures. Under this assumption, based, for example, on the pair of distances between NeuAc $H3_{ax}$–Gal H6R and NeuAc $H3_{ax}$–Gal H6S (Table 3), we arrived at a population ratio p_I:p_{II} close to 0.9:0.1. On the other hand, if the rate of interconversion between structures **I** and **II** is on the order of that for molecular tumbling or greater, averaging of relaxation parameters occurs at the level of relaxation theory when calculating spectral density functions (Wennerström, 1972; Tropp, 1980). In this case, both radial and angular averaging of NOE effects must be taken into account, which would result in a population of type **II** structures significantly higher than for a slow interconversion situation. However, since we obtained such a good match between virtually all experimental parameters and MMC simulation results for type **I** structures (see Table 3), we favor the first possibility.

Our GEGOP Monte-Carlo computer simulations are known to overestimate the free energy barrier between the two types of structures. However, the reason the population of type **I** structures is underestimated by the simulations is not clear. A possible explanation might be that hydro-

gen bonding terms are not explicitly taken into account in the HSEA model. To incorporate appropriate hydrogen-bond potentials into the force field is not easy since the current parameterization of the Van der Waals interactions was obtained in part from data on crystals where hydrogen bonds are present. Although our calculations apparently underestimate hydrogen bonds, including hydrogen-bond potentials into in-vacuo parameterizations can easily lead to overestimation of their effects (Cumming and Carver, 1987; Carver et al., 1990).

The model for S6L in structure **I** (Fig. 12a) shows a large hydrophobic patch formed by the protons of all 3 residues. Such a large hydrophobic surface can only arise in this particular conforma-

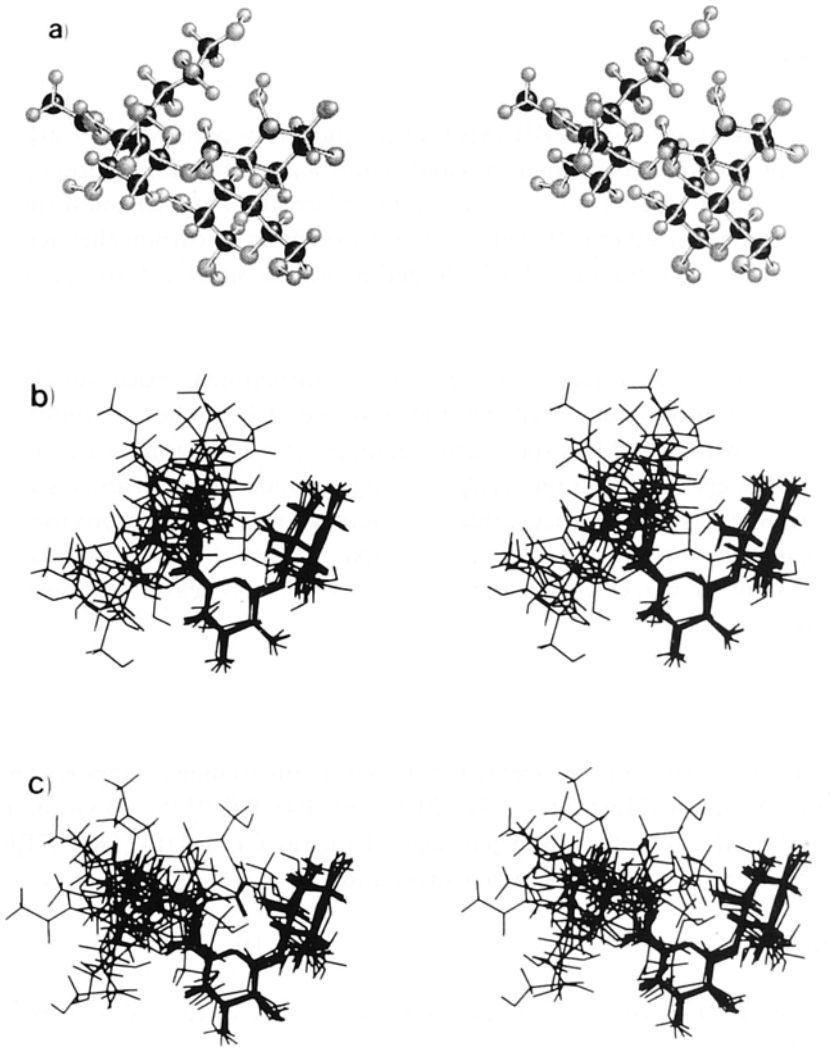

Fig. 12. (a) Stereoplots of the minimum-energy 'family **I**' conformer of sialyl-α(2→6)-lactose (with $\Phi_{2,6} = -60°$) in aqueous solution. The ball-and-stick model clearly shows the long-range NeuAc OH7:::Glc OH3 hydrogen bond. (b) Stereoplots of 10 overlayed 'family **I**' structures of S6L (with $\Phi_{2,6} = -60°$) as obtained from MMC simulations at 800 K. (c) Stereoplots of 10 overlayed 'family **II**' structures of S6L (with $\Phi_{2,6} = 180°$), to illustrate the flexibility around the (2→6)-linkage associated with the lack of the interresidue NeuAc OH7:::Glc OH3 hydrogen bond.

tion; it is often thought to be responsible for molecular recognition phenomena (Lemieux, 1989; Ben-Naim et al., 1990). The hydrophilic groups, such as the carboxylic function of NeuAc and the C6 hydroxymethyl group of the Glc residue in the *gg* position, both of which are located on the peripherals of the surface in structures **I** (Fig. 12b), may 'lock' this conformation by hydrogen-bond interactions when bound to a receptor. Alternatively, S6L may unfold from structures **I** to structures **II** (Fig. 12c) upon binding to a protein receptor, driven by the opportunity to form a larger number of hydrogen-bond interactions with the protein. The elucidation of the binding mechanism of S6L to various receptors and the comparison of the structures of S6L determined here for the free oligosaccharide and that bound to a receptor are the subject of current studies in our laboratory.

CONCLUSIONS

On the basis of high-resolution NMR experiments and Metropolis Monte Carlo simulations, we predicted the predominant conformations and conformational flexibility of sialyl-α(2→6)-lactose in aqueous solution. The most crucial structural information was gained from spectroscopy of the hydroxyl protons, together with deuterium isotope effects on carbon chemical shifts, showing the existence of stable intramolecular hydrogen bonds for sialyl-α(2→6)-lactose in aqueous solution. The large number (>25) of NMR constraints found in the present study of sialyl-α(2→6)-lactose made feasible careful comparison between experimental and simulated parameters. The importance of adequate sampling of the conformational space was clearly illustrated. The force field used in our study predicted the existence of 2 families of conformers that agree semiquantitatively with the NMR experimental findings. Our findings for sialyl-α(2→6)-lactose in aqueous solution suggest that intramolecular hydrogen bonds may contribute significantly to the conformational stability of oligosaccharides in solution. Inclusion of appropriate terms for hydrogen bonds into the force-field calculations (compare Jeffrey, 1990, and Rees and Smith, 1975) should further improve agreement between the results of theoretical calculations and NMR-derived structures.

ACKNOWLEDGEMENTS

Thanks are due to Mr. D.L. Warrenfeltz for continuous technical support. This research was supported by US National Institutes of Health Grants P41-RR-05351 (Division of Research Resources) and P01-AI-27135, the US Department of Energy Grant DE-FG09-87ER13810, and an equipment grant from Digital Equipment Corporation.

REFERENCES

Acquotti, D., Poppe, L., Dabrowski, J., Von der Lieth, C.W., Sonnino, S. and Tettamanti, G. (1990) *J. Am. Chem. Soc.*, **112**, 7772–7778.

Bax, A. (1988) *J. Magn. Reson.*, **77**, 134–147.

Bax, A. and Davis, D.G. (1985) *J. Magn. Reson.*, **63**, 207–213.

Ben-Naim, A., Ting, K.L. and Jernigan, R.L. (1990) *Biopolymers*, **29**, 901–919.

Berman, E. (1984) *Biochemistry*, **23**, 3754–3759.

Bock, K. (1983) *Pure Appl. Chem.*, **55**, 605–622.

Bothner-By, A.A. and Shukla, R. (1988) *J. Magn. Reson.*, **77,** 524–535.
Bothner-By, A.A., Stephens, R.L., Lee, J., Warren, C.D. and Jeanloz, R.W. (1984) *J. Am. Chem. Soc.*, **106,** 428–429.
Boudot, D., Canet, D., Brondeau, J. and Boubel, J.C. (1989) *J. Magn. Reson.*, **83,** 428–439.
Brady, J.W. (1989) *J. Am. Chem. Soc.*, **111,** 5155–5165.
Braunschweiler, L. and Ernst, R.R. (1983) *J. Magn. Reson.*, **53,** 521–528.
Breg, J., Kroon-Batenburg, L.M.J., Strecker, G., Montreuil, J. and Vliegenthart, J.F.G. (1989) *Eur. J. Biochem.*, **178,** 727–739.
Brown, E.B., Brey, W.S. and Weltner, W.Jr. (1975) *Biochim. Biophys. Acta*, **399,** 124–130.
Bush, C.A. (1988) *Bull. Magn. Reson.*, **10,** 73–95.
Carver, J.P., Mandel, D., Michnick, S.W., Imberty, A. and Brady, J.W. (1990) *ACS Symp. Ser.*, **430,** 266–280.
Casu, B., Reggiani, M., Gallo, G.G. and Vigevani, A. (1966) *Tetrahedron*, **22,** 3061–3083.
Christofides, J.C., Davies, D.B., Martin, J.A. and Rathbone, E.B. (1986) *J. Am. Chem. Soc.*, **108,** 5738–5743.
Chu, S.S.C. and Jeffrey, G.A. (1968) *Acta Crystallogr., Sect. B*, **24,** 830–838.
Cumming, D.A. and Carver, J.P. (1987) *Biochemistry*, **26,** 6676–6683.
Dabrowski, J. and Poppe, L. (1989) *J. Am. Chem. Soc.*, **111,** 1510–1511.
Edge, C.J., Singh, U.C., Bazzo, R., Taylor, G.L., Dwek, R.A. and Rademacher, T.W. (1990) *Biochemistry*, **29,** 1971–1974.
Farmer, B.T., II, Macura, S. and Brown, L.R. (1987) *J. Magn. Reson.*, **72,** 347–352.
Fejzo, J., Zolnai, Z., Macura, S. and Markley, J.L. (1989) *J. Magn. Reson.*, **82,** 518–528.
French, A.D. (1988) *Biopolymers*, **27,** 1519–1525.
Geen, H., Wu, X.L., Friedrich, J. and Freeman, R. (1989) *J. Magn. Reson.*, **81,** 646–652.
Ha, S.N., Giammona, A., Field, M. and Brady, J.W. (1988) *Carbohydr. Res.*, **180,** 207–221.
Haasnoot, C.A.G., De Leeuw, F.A.A.M. and Altona, C. (1980) *Tetrahedron*, **36,** 2783–2792.
Hills, B.P. (1991) *Mol. Phys.*, **72,** 1099–1121.
Homans, S.W. (1990a) *Progr. NMR Spectrosc.*, **22,** 55–81.
Homans, S.W. (1990b) *Biochemistry*, **29,** 9110–9118.
Homans, S.W., Dwek, R.A., Boyd, J., Mahmoudian, M., Richards, W.G. and Rademacher, T.W. (1986) *Biochemistry*, **25,** 6342–6350.
Homans, S.W., Dwek, R.A. and Rademacher, T.W. (1987) *Biochemistry*, **26,** 6571–6578.
Hoult, D.J. and Richards, R.E. (1975) *Proc. Royal Soc. London*, **344,** 311–319.
Imberty, A., Gerber, S., Tran, V. and Pérez, S. (1990) *Glycoconjugate J.*, **7,** 27–54.
Jeffrey, G.A. (1990) *ACS Symp. Ser.*, **430,** 20–30.
Karplus, M. (1959) *J. Chem. Phys.*, **30,** 11–15.
Kessler, H., Gemmecker, G. and Haase, B. (1988) *J. Magn. Reson.*, **77,** 401–408.
Lemieux, R.U. (1989) *Chem. Soc. Rev.*, **18,** 347–374.
Lemieux, R.U. and Bock, K. (1984) *Jpn. J. Antibiot. Suppl.*, **32,** 163–167.
Lemieux, R.U., Bock, K., Delbaere, L.T.J., Koto, S. and Rao, V.S. (1980) *Can. J. Chem.*, **58,** 631–653.
Lerner, L. and Bax, A. (1987) *Carbohydr. Res.*, **166,** 35–46.
Marion, D. and Wüthrich, K. (1983) *Biochem. Biophys. Res. Commun.*, **113,** 967–974.
Metropolis, N., Rosenbluth, A.W., Rosenbluth, M.N., Teller, A.H. and Teller, E. (1953) *J. Chem. Phys.*, **21,** 1087–1092.
Meyer, B. (1990) *Top. Curr. Chem.*, **154,** 141–208.
Meyer, B., Zsiska, M. and Stuike-Prill, R. (1992) In *Computer Simulation Studies in Condensed Matter Physics* (Eds. Landau, D.P., Mon, K.K. and Schuttler, H.B.) Vol. IV, Springer, Heidelberg, in press.
Morris, G.A. and Freeman, R. (1978) *J. Magn. Reson.*, **29,** 433–462.
Müller, L. (1979) *J. Am. Chem. Soc.*, **101,** 4481–4482.
Mulloy, B., Frenkiel, T.A. and Davies, D.B. (1988) *Carbohydr. Res.*, **184,** 39–46.
Neuhaus, D. and Williamson, M.P. (1989) *The Nuclear Overhauser Effect in Structural and Conformational Analysis*, VCH Publishers, New York.
Ohrui, H., Nishida, Y., Watanabe, M., Hori, H. and Meguro, H. (1985) *Tetrahedron Lett.*, **26,** 3251–3254.
Ohrui, H., Nishida, Y., Itoh, H. and Meguro, H. (1991) *J. Org. Chem.*, **56,** 1726–1731.
Otting, G. and Wüthrich, K. (1988) *J. Magn. Reson.*, **76,** 569–574.
Peters, T., Meyer, B., Stuike-Prill, R., Somorjai, R. and Brisson, J.R. (1992) *Biochemistry*, in press.
Platzer, N., Davoust, D., Lhermitte, M., Bauvy, C., Meyer, D.M. and Derappe, C. (1989) *Carbohydr. Res.*, **191,** 191–207.

Poppe, L. and Dabrowski, J. (1989) *Biochem. Biophys. Res. Commun.*, **159**, 618–623.
Poppe, L., Dabrowski, J., Von der Lieth, C.W., Numata, M. and Ogawa, T. (1989) *Eur. J. Biochem.*, **180**, 337–342.
Poppe, L., Von der Lieth, C.W. and Dabrowski, J. (1990a) *J. Am. Chem. Soc.*, **112**, 7762–7771.
Poppe, L., Dabrowski, J., Von der Lieth, C.W., Koike, K. and Ogawa, T. (1990b) *Eur. J. Biochem.*, **189**, 313–325.
Poppe, L. and Van Halbeek, H. (1991a) *J. Am. Chem. Soc.*, **113**, 363–365.
Poppe, L. and Van Halbeek, H. (1991b) *Magn. Reson. Chem.*, **29**, 355–361.
Poppe, L. and Van Halbeek, H. (1991c) *J. Magn. Reson.*, **92**, 636–641.
Poppe, L. and Van Halbeek, H. (1991d) *J. Magn. Reson.*, **93**, 214–217.
Poppe, L. and Van Halbeek, H. (1991e) *Magn. Reson. Chem.*, **29**, 848–851.
Poppe, L. and Van Halbeek, H. (1991f) *Glycoconjugate J.*, **8**, 130.
Rademacher, T.W., Parekh, R.B. and Dwek, R.A. (1988) *Annu. Rev. Biochem.*, **57**, 785–838.
Ram, P., Mazzola, L. and Prestegard, J.H. (1989) *J. Am. Chem. Soc.*, **111**, 3176–3182.
Rasmussen, K. (1983) *J. Mol. Struct.*, **97**, 53–56.
Rees, D.A. and Smith, P.J.C. (1975) *J. Chem. Soc. Perkin II*, 830–835.
Reuben, J. (1984) *J. Am. Chem. Soc.*, **106**, 6180–6186.
Scarsdale, J.N., Ram, P., Prestegard, J.H. and Yu, R.K. (1988) *J. Comput. Chem.*, **9**, 133–147.
Schauer, R. (1982) *Adv. Carbohydr. Chem. Biochem.*, **40**, 131–234.
Sklenar, V. and Bax, A. (1987) *J. Am. Chem. Soc.*, **74**, 469–479.
Sklenar, V. and Feigon, J. (1990) *J. Am. Chem. Soc.*, **112**, 5644–5645.
Spoormaker, T. and De Bie, M.J.A. (1978) *Recl. Trav. Chim. Pays-Bas*, **97**, 61–90.
Stuike-Prill, R. and Meyer, B. (1990) *Eur. J. Biochem.*, **194**, 903–919.
Stuike-Prill, R. and Meyer, B. (1991) *Carbohydr. Res.*, submitted.
Subramanian, S. and Bax, A. (1987) *J. Magn. Reson.*, **71**, 325–330.
Thøgersen, H., Lemieux, R.U., Bock, K. and Meyer, B. (1982) *Can. J. Chem.*, **60**, 44–57.
Tropp, J. (1980) *J. Chem. Phys.*, **72**, 6035–6047.
Tvaroska, I., Hricovini, M. and Petráková, E. (1989) *Carbohydr. Res.*, **189**, 359–362.
Tvaroska, I. (1990) *Carbohydr. Res.*, **206**, 55–64.
Van Halbeek, H. and Poppe, L. (1991) *Abstr. 10th International Meeting on NMR Spectroscopy*, St. Andrews, Scotland, July 8–12, 1991, p. O 10.
Wennerström, H. (1972) *Mol. Phys.*, **24**, 69–80.
Wiberg, K.B. and Murcko, M.A. (1989) *J. Am. Chem. Soc.*, **111**, 4821–4828.
Wu, X.L., Xu, P., Friedrich, J. and Freeman, R. (1989) *J. Magn. Reson.*, **81**, 206–211.
Wüthrich, K. (1986) *NMR of proteins and nucleic acids*, Wiley, New York.
Yan, Z.Y. and Bush, C.A. (1990) *Biopolymers*, **29**, 799–811.